



Connectivity-based Meta-Bands: A new approach for automatic frequency band identification in connectivity analyses

Víctor Rodríguez-González ^{a,b,*}, Pablo Núñez ^{a,b,c}, Carlos Gómez ^{a,b}, Yoshihito Shigihara ^d, Hideyuki Hoshi ^d, Miguel Ángel Tola-Arribas ^{b,e}, Mónica Cano ^e, Ángel Guerrero ^{f,g}, David García-Azorín ^f, Roberto Hornero ^{a,b,h}, Jesús Poza ^{a,b,h}

^a Biomedical Engineering Group, University of Valladolid, Valladolid, Spain

^b Centro de Investigación Biomédica en Red de Bioingeniería, Biomateriales y Nanomedicina, Instituto de Salud Carlos III (CIBER-BBN), Spain

^c Coma Science Group, GIGA-Consciousness, University of Liège, Liège, Belgium

^d Hokuto Hospital, Obihiro, Japan

^e Servicio de Neurología. Hospital Universitario Río Hortega, Valladolid, Spain

^f Hospital Clínico Universitario, Valladolid, Spain

^g Department of Medicine, University of Valladolid, Spain

^h IMUVA, Instituto de Investigación en Matemáticas, University of Valladolid, Spain

ARTICLE INFO

Keywords:

Functional network
Louvain community detection
Frequency bands
Connectivity-based Meta-Bands
Automatic and personalized frequency band segmentation

ABSTRACT

The majority of electroencephalographic (EEG) and magnetoencephalographic (MEG) studies filter and analyse neural signals in specific frequency ranges, known as “canonical” frequency bands. However, this segmentation, is not exempt from limitations, mainly due to the lack of adaptation to the neural idiosyncrasies of each individual. In this study, we introduce a new data-driven method to automatically identify frequency ranges based on the topological similarity of the frequency-dependent functional neural network. The resting-state neural activity of 195 cognitively healthy subjects from three different databases (MEG: 123 subjects; EEG₁: 27 subjects; EEG₂: 45 subjects) was analysed. In a first step, MEG and EEG signals were filtered with a narrow-band filter bank (1 Hz bandwidth) from 1 to 70 Hz with a 0.5 Hz step. Next, the connectivity in each of these filtered signals was estimated using the orthogonalized version of the amplitude envelope correlation to obtain the frequency-dependent functional neural network. Finally, a community detection algorithm was used to identify communities in the frequency domain showing a similar network topology. We have called this approach the “Connectivity-based Meta-Bands” (CMB) algorithm. Additionally, two types of synthetic signals were used to configure the hyper-parameters of the CMB algorithm. We observed that the classical approaches to band segmentation are partially aligned with the underlying network topologies at group level for the MEG signals, but they are missing individual idiosyncrasies that may be biasing previous studies, as revealed by our methodology. On the other hand, the sensitivity of EEG signals to reflect this underlying frequency-dependent network structure is limited, revealing a simpler frequency parcellation, not aligned with that defined by the “canonical” frequency bands. To the best of our knowledge, this is the first study that proposes an unsupervised band segmentation method based on the topological similarity of functional neural network across frequencies. This methodology fully accounts for subject-specific patterns, providing more robust and personalized analyses, and paving the way for new studies focused on exploring the frequency-dependent structure of brain connectivity.

1. Introduction

The brain is the most complex biological system of the human body (Fan, 2021). It is composed by a myriad of neurons continuously communicating by synapses. There are many neuroimaging techniques

that allow the acquisition of the electromagnetic activity generated by these synapses, such as electroencephalography (EEG) and magnetoencephalography (MEG). These neurophysiological techniques have a high temporal resolution (in the order of milliseconds). This enables the

* Corresponding author at: Biomedical Engineering Group, University of Valladolid, Valladolid, Spain.

E-mail address: victor.rodriguez@gib.tel.uva.es (V. Rodríguez-González).

<https://doi.org/10.1016/j.neuroimage.2023.120332>

Received 2 April 2023; Received in revised form 5 July 2023; Accepted 14 August 2023

Available online 22 August 2023

1053-8119/© 2023 The Author(s). Published by Elsevier Inc. This is an open access article under the CC BY-NC-ND license (<http://creativecommons.org/licenses/by-nc-nd/4.0/>).

capture of faster brain activity, which is of great interest in a dynamic system as the brain (Babiloni et al., 2009). EEG and MEG (M/EEG) also have relevant differences between them: while EEG has a reduced cost, portability, and is more widespread in clinical settings (Poza et al., 2017), MEG is contactless, and more robust against volume conduction effects (Rampp and Stefan, 2007; van den Broek et al., 1998). Furthermore, although both techniques record the same sources, EEG is sensitive to radial and tangential sources, whereas MEG is only sensitive to the latter ones (Ahlfors et al., 2010). It has been proposed to combine both acquisition techniques to optimize the information obtained and increase the spatial resolution of the recordings (Rampp and Stefan, 2007; Molins et al., 2008; Malmivuo, 2012).

There are many ways of analysing M/EEG signals. One such way is by individually assessing the time course of each sensor or brain region. In this way, we can obtain information about the behaviour of individual neuronal groups, what is known as “local activation” analyses (Stam and van Straaten, 2012). Nonetheless, by analysing only the local patterns we are losing lots of information. It is noteworthy that neurons interact between them, forming dynamical networks that emerge via chemical and electrical processes (Tognoli and Kelso, 2014; Núñez et al., 2021). Different brain regions are involved in these networks, whose interactions support higher cognitive functions, such as deduction or reasoning (Vohryzek et al., 2020). There is a huge amount of studies devoted to assess these interactions (O’Neill et al., 2018), which are known as “functional connectivity” (FC) analyses (Colclough et al., 2016; Bastos and Schoffelen, 2016; Boon et al., 2021; Briels et al., 2020; Miraglia et al., 2017; O’Reilly et al., 2017).

Although there are sophisticated multi-dimensional methodological approaches to estimate the FC that do not require the segmentation of neural activity in frequency bands (Basti et al., 2020; Rahimi et al., 2023), it is noteworthy that FC studies typically analyse the neural interactions in specific frequency ranges: the well-known “canonical” frequency bands (i.e., delta, theta, alpha, beta-1, beta-2, and gamma). These bands are supported by abundant literature, and they reflect certain brain patterns with extensively proved physiological meaning (Sanei and Chambers, 2021; Uhlhaas et al., 2008). Moreover, as canonical frequency bands are widespread, they provide a common framework that ease the comparisons across subjects and studies. However, there are several issues related with their definition: (i) they were specified about 80 years ago, when the techniques for the acquisition of neural activity were remarkably different than those currently available (Jasper and Andrews, 1936, 1938; Berger, 1934; Walter, 1936; Walter and Dovey, 1944); (ii) there is a noticeable inconsistency in their definition, with different band boundaries across studies (Newson and Thiagarajan, 2019); (iii) most of the current analysis methods, such as FC, had not been developed when the canonical frequency bands were introduced and, as a consequence, they were defined based on local activation patterns, thus losing relevant features of the neural signals; and (iv) the canonical frequency bands do not account for individual idiosyncrasies at subject-level. Other approaches to frequency band segmentation tried to address the latter issue, proposing subject-adaptive frequency bands (Pascarelli et al., 2020; Borghini et al., 2019). These methods assess the distribution of the spectral content of the signals to specify the personalized frequency band boundaries and, consequently, they also rely on local activation patterns (Pascarelli et al., 2020; Borghini et al., 2019). In this way, they take into account some of the individual idiosyncrasies, but a great level of homogenization is still present, as they use fixed parameters such as the number of bands or their bandwidth. FC patterns reflect the global interaction between brain regions, but also the local synchronization, thus summarizing a richer variety of neural properties (Rodríguez-González et al., 2021; Tewarie et al., 2019a). Hence, it is reasonable to consider whether an alternative, automatic, FC-based, and subject-specific frequency band segmentation can be appropriate.

As we have mentioned, the majority of FC studies using M/EEG employ frequency bands with fixed frequency ranges. This could be

a confounding factor, as it can be hiding relevant results by grouping frequencies with very different connectivity features (Newson and Thiagarajan, 2019). In this paper, we propose, to the best of our knowledge, the first methodology that allows to find unsupervised data-driven frequency bands based on the connectivity topology. The methodology proposed here automatically groups frequency bins based on the topological similarity between them. We have called this new methodology the “Connectivity-based Meta-Bands” (CMB) algorithm. Throughout this paper, the term meta-band is used to name the frequency ranges that our methodology identifies as belonging to the same community based on their network topology. The CMB algorithm allows to perform connectivity analyses accounting for the underlying frequency structure, thus having personalized analyses that fully adapt to the individual idiosyncrasies of neural activity of each subject.

Based on the hypothesis that we can automatically define user-specific frequency ranges to be used in connectivity analyses, the following research questions are posed in the manuscript: (i) how is the topology of the underlying frequency-dependent neural network structure? and (ii) can we define adaptive frequency bands that are a better fit for this network structure than canonical frequency bands? To answer these questions, the main objective of this paper is to develop a FC-based, unsupervised, and subject-specific frequency band segmentation approach. This would allow to perform subsequent analyses without the bias factor of considering the frequency bands to be fixed across subjects.

2. Materials

2.1. Synthetic signals

In order to assess the performance of the methodology under controlled conditions, it was tested using synthetic signals with known ground-truth. Two different types of signals were used: (i) amplitude-coupled synthetic signals, and (ii) M/EEG-like synthetic signals.

2.1.1. Amplitude-coupled synthetic signals

These signals were designed to gain a better understanding of the performance of the methodology, as well as to define its limitations while keeping the computational burden in an acceptable level. Three minutes of activity in 20 channels were generated with a sampling frequency of 1000 Hz, and segmented in 5 s epochs. As the signals were stationary, we considered that 3 min of activity was enough for a proper operation of the CMB algorithm. These signals were used to assess the influence of different hyper-parameters on the results, which will be defined below: filter order, sampling frequency, bandwidth, band overlapping, and frequency resolution.

These signals were generated by means of an amplitude modulation (AM) in specific frequency ranges and channels (that determined our underlying meta-bands), and a low level of white Gaussian noise in the broadband (−19 dBW). The final signal, $s(t)$, in each sensor i was constructed as follows:

$$s_i(t) = x(t) \cdot w_i + o(t), \quad (1)$$

where $x(t)$ is the modulated signal (Eq. (2)), w_i the binary weight used to construct the underlying connectivity matrix for each sensor i , and $o(t)$ a white Gaussian noise signal. In this way, $x(t)$ is the same for all the sensors, while the coupling is determined by w_i , with “1” indicating coupling, and “0” not coupling. The AM signal $x(t)$ is defined as follows:

$$x(t) = A_c \cdot [1 + k_a \cdot m(t)] \cdot \cos(2\pi f_c t), \quad (2)$$

where A_c is the carrier amplitude, k_a the modulation index, $m(t)$ the modulating signal, and f_c the carrier frequency. Finally, the modulating signal $m(t)$ is defined as:

$$m(t) = \sum_{n=1}^l \cos(2\pi f_n t), \quad (3)$$

with l being the number of cosines composing the signal, and f_n the frequency of each cosine. Thus, by varying f_c , f_n and l , we can obtain signals with the AM in different frequencies and with different bandwidths. In the simulated scenarios where more than two AM are required, the two signals are summed, *i.e.* $s_i(t) = s_{i1}(t) + s_{i2}(t)$. Further details on the generation of these signals can be found in section 1.1 of the Supplementary Material.

2.1.2. M/EEG-like synthetic signals

To evaluate the performance of the CMB algorithm with signals closer to brain physiological time courses, M/EEG-like synthetic signals were generated. These signals contain a similar data distribution to that of real M/EEG recordings, thus providing a more realistic scenario. Nonetheless, they have an increased computational burden compared to the amplitude-coupled synthetic signals. These signals have the same number of neural sources as the original M/EEG signals (*i.e.*, 68 neural sources), the same duration in time, and are also divided into 5 s epochs.

We employed 5 real source-level MEG recordings as the basis to create these signals. First of all, we took advantage of surrogate data testing to eliminate the static FC interactions from the 5 recordings (Hindriks et al., 2016; Stam, 2006). Specifically, we used the amplitude adjusted Fourier transform (AAFT), which is an improved version of the phase randomization method of surrogate data construction which preserves the amplitude distribution of the data (Prichard and Theiler, 1994; Khambhati et al., 2018). This algorithm is capable of destroying the static FC of a time series while preserving the amplitude distribution and the linear structure of the data (Hindriks et al., 2016; Stam, 2006). That is, after applying AAFT, we have 5 synthetic M/EEG-like signals similar to the original ones, but with a negligible degree of static FC between them. Then, the coupling between these signals (*i.e.*, the FC) was generated by means of filtering and weighted summing processes in specific frequency ranges. The resulting signals have non-negligible FC only in the defined frequency ranges.

These synthetic signals were used to gain deeper insights on how the sampling frequency affects the meta-bands. In addition, we employed these signals to find out whether our methodology is capable of recovering, at least, 6 underlying bands with and without a gap with negligible FC between them (see Section 3.3). More details about the generation of these signals can be found in section 1.2 of the Supplementary Material.

2.2. Real M/EEG recordings

The CMB algorithm was also applied to analyse neural activity of a cohort of 195 subjects from three different databases: 123 from an MEG database, and 27 and 45 for two independent EEG databases. For all the databases, 5 min of resting-state eyes-closed brain activity were recorded. All patients were asked to remain awake and still during the recordings. The neural activity was monitored in real time to prevent subjects from falling asleep (Núñez et al., 2021; Rodríguez-González et al., 2019). All the subjects included in the study had no history of neurological or psychiatric disorders. In addition, they did not take medication that could have an influence on M/EEG activity. Although the CMB algorithm can also be applied to task-related paradigms, their dynamical characteristics require further considerations on the CMB algorithm that should be addressed in future studies, as they increase the complexity of the required tests. Thus, we decided to employ the simplest paradigm, based on considering resting-state recordings, to provide the initial evaluation of the method. Furthermore, the resting-state paradigm is widely used by the scientific community to study intrinsic brain behaviour and neural alterations associated with different pathologies (Boon et al., 2019; Cassani et al., 2018; Newson and Thiagarajan, 2019). Hence, this paradigm is useful in clinical setting in which other protocols are difficult to apply (or even impossible), for example with patients suffering from dementia.

2.2.1. Characteristics of M/EEG recordings

MEG activity was recorded from 123 cognitively healthy controls using a 160-channel axial gradiometer MEG system (MEG Vision PQ1160C, Yokogawa Electric, sampling rate 1000 Hz). The sample is composed of 61 females and 62 males with an age of 48.3 ± 16.1 years (mean \pm standard deviation, SD).

The first EEG database (EEG₁) was comprised by 27 healthy females. Neural signals were recorded with a 32-channel EEG system (actiChamp Plus, BrainVision) at the Clinical University Hospital, Valladolid (Spain) and at the Institute for Research & Innovation in Health of the Porto University (Portugal). The electrodes were placed according to the 10–20 system using a common reference: C3, C4, Cz, CP1, CP4, CP5, CP6, F3, F4, F7, F8, Fz, FC1, FC2, FC5, FC6, Fp1, Fp2, FT9, FT10, O1, O2, Oz, P3, P4, P7, P8, Pz, T7, T8, TP9, TP10. The age of the sample was 30.8 ± 6.6 years (mean \pm SD).

The EEG activity of the second EEG database (EEG₂) was recorded from 45 cognitively healthy elderly controls. Brain activity was recorded with a 19-channel EEG system (XLTEK[®], Natus Medical) at the Department of Clinical Neurophysiology of the “Río Hortega” University Hospital, Valladolid, Spain. Electrodes were placed according to the international 10–20 system using a common average reference: Fp1, Fp2, Fz, F3, F4, F7, F8, Cz, C3, C4, T3, T4, T5, T6, Pz, P3, P4, O1, and O2. The sample was composed by 31 females and 14 males, with an age of 76.3 ± 4.0 years (mean \pm SD).

All the studies were conducted according to the Code of Ethics of the World Medical Association (Declaration of Helsinki). The Ethics Committee of the Hokuto Hospital (Obihiro, Japan) approved the study for the MEG database (code #1001 and #1038); the Ethics Committee of the Clinical University Hospital (Valladolid, Spain) and Institute for Research & Innovation in Health (Porto, Portugal) approved the study for the EEG₁ database (codes PI19-1531 and 5/CECRI/2020); and the Ethics Committee of the “Río Hortega” University Hospital (Valladolid, Spain) approved the study for the EEG₂ database (code 36/2014/02). All participants and caregivers were informed about the research and study protocol and gave their written informed consent.

2.2.2. Preprocessing of the M/EEG recordings

A similar preprocessing pipeline was conducted for the three databases (Rodríguez-González et al., 2020): (i) filtering the signals with two finite impulse response filters: a band-pass filter to limit noise bandwidth (1–70 Hz) and a band-stop filter (49–51 Hz) to remove powerline noise; (ii) independent component analysis to remove artefactual components, by means of the Infomax algorithm, to visually identify and remove components related with artefacts, and (iii) visual selection of 5 s artefact-free epochs. For the MEG database 5.2 ± 3.2 (mean \pm standard deviation) ICA components were rejected and 9.0 ± 6.3 epochs were visually discarded. Also, for the EEG₁ database 6.7 ± 3.7 ICA components were rejected and 13.9 ± 8.1 epochs were visually discarded. Finally, for the EEG₂ database 3.0 ± 2.0 ICA components were rejected and 14.4 ± 7.4 epochs were visually discarded.

Additionally, the increased number of sensors of the MEG recordings allowed the application of an additional artefact rejection step (the SOUND algorithm Rodríguez-González et al., 2019; Mutanen et al., 2018) before the filtering. This algorithm was applied using an anatomical template and a $\lambda_0 = 0.1$, according to the values suggested in a previous study (Rodríguez-González et al., 2019).

2.2.3. Source reconstruction

MEG and EEG time series were reconstructed at source-level using the Weighted Minimum Norm Estimation (wMNE) method (Lin et al., 2006). This algorithm restricts the sources of the inverse problem by minimizing the energy (l_2 norm) while weighting deep sources to facilitate their detection (Lin et al., 2006). This algorithm was selected as it is widely used in the context of MEG and EEG source localization (Rodríguez-González et al., 2020; Tait et al., 2021; Rizkallah et al., 2020; Larson-Prior et al., 2013). Of note, it can be argued that a more

appropriate source inversion algorithm could be selected for a specific signal modality (as example, sLORETA for EEG (Pascual-Marqui, 2002)). However, in this study the source inversion process is not intended to unveil the real underlying sources, but to establish a common space for all three databases, while keeping their processing pipelines as similar as possible. The wMNE implementation is freely available in Brainstorm toolbox (<http://neuroimage.usc.edu/brainstorm>) (Tadel et al., 2011).

An anatomical forward model was created using the ICBM152 template (Fonov et al., 2009; Douw et al., 2018). Based on it, a three-layer (brain, skull, and scalp) realistic head model was generated with a boundary element method using the OpenMEEG software (Rodríguez-González et al., 2020; Gramfort et al., 2010). The source space was limited to the cortex using a total number of 15000 sources (Rodríguez-González et al., 2020). The sources were restricted to be normal to the cortex (Rodríguez-González et al., 2020). Finally, after flipping the sources of opposite direction to avoid blurring of neighbouring generators (Vidaurre et al., 2016), the 15000 sources were grouped in the 68 regions of interest (ROIs) according to the Desikan–Killiany atlas (Rodríguez-González et al., 2020; Desikan et al., 2006; Lai et al., 2018).

3. Methods: Connectivity-based meta-bands

3.1. Computation of the functional networks

Preprocessed source-level time signals were used to estimate the functional networks. In Fig. 1 the analysis steps of the study are illustrated. Further details on the filtering process, and the estimation of the connectivity are included in subsequent sections. The steps carried out to build them are summarized below.

- (i) Define the algorithm parameters (filter order, sampling frequency, frequency resolution, filter boundaries, etc.).
- (ii) Z-score transform the signals.
- (iii) Filter the signals with a narrow bandwidth.
- (iv) Orthogonalize the signals.
- (v) Estimate the connectivity by means of the amplitude envelope correlation (AEC).
- (vi) Repeat steps 3–5 for each of the frequency ranges defined in step 1. The resulting matrices have the following dimensions: $N \times M \times M \times Q$, where N is the number of frequency bins, M the number of sources, and Q the number of epochs.
- (vii) Extract communities across the frequency dimension by means of the Louvain GJA algorithm. These frequency-dependent communities are what we refer to as meta-bands.

Although the operation of the CMB algorithm is considered unsupervised, some parameters were tuned during the algorithm development. To this end, we took advantage of the synthetic signals previously described (both amplitude-coupled and M/EEG-like). Of note, although the algorithm displays satisfactory performance with the default parameters, they can be modified depending on the user requirements, such as lower computational burden or different frequency range of interest.

3.1.1. Filtering process

A narrow-band filter bank was employed to filter the signals, employing a Hamming window to minimize the filter ripple (Cohen, 2014). The MATLAB *filtfilt* function was used to achieve a filtering process with no phase distortion (Cohen, 2014). Furthermore, to avoid the edge effect of the filter, the filtering process was performed considering the whole recording (before the segmentation into 5 s epochs); in addition, the first and last 5 s epochs of the synthetic and real signals were discarded to avoid the influence of filter transient effects in the results (Cohen, 2014). Different filter orders were assessed to evaluate the algorithm performance (namely 100, 250, 500, 750,

1000, 1250, 1500, 2000, 2500, and 3000). Additionally, the filtering process was carried out with a 50% overlap between filters to increase the frequency resolution and smooth the evolution of the frequency-dependent networks.

3.1.2. Connectivity estimation: orthogonalized amplitude envelope correlation

The selection of the connectivity metric is a decision of utmost importance for the application of the CMB algorithm, as different connectivity metrics are likely sensitive to different aspects of brain dynamics (He et al., 2019; Schoonhoven et al., 2022). Several reasons led us to consider the orthogonalized version of the AEC. Firstly, thanks to the orthogonalization process, this metric is robust against volume conduction and field spread effects, which are major confounding factors in connectivity analyses (Colclough et al., 2016). Additionally, it has been proven to be robust and consistent, displaying a high level of reproducibility and repeatability; these features have been previously considered as quality markers for connectivity metrics (Colclough et al., 2016; Schoonhoven et al., 2022). Also, as the mathematical formulation of the AEC is simple, it is easier to interpret than other more mathematically convoluted parameters (Brookes et al., 2014; Colclough et al., 2016). Furthermore, it is sensitive to the alterations of neurological disorders in functional connectivity, which is relevant for future potential clinical implementations of the CMB algorithm (Schoonhoven et al., 2022). Finally, amplitude-based metrics have been adapted to compute instantaneous connectivity patterns, which have been successfully used to identify brain states from electrophysiological signals (Núñez et al., 2021, 2022; Tewarie et al., 2019b).

The AEC is an amplitude-based connectivity metric (Brookes et al., 2014). To calculate the AEC, the power envelope of the signals is computed as the absolute value of the Hilbert transform. Finally, the AEC is calculated as the Pearson correlation between the two signal envelopes. This metric was used due to its robustness, simplicity, and consistency across studies (Colclough et al., 2016; Schoonhoven et al., 2022). Before computing the AEC, a pairwise orthogonalization was applied to the signals in order to avoid spurious correlations due to volume conduction and field spread effects (Brookes et al., 2012). The AEC is used to obtain the frequency-dependent connectivity matrices of the filtered signals from the previous step. Before performing the community detection, the connectivity matrices of all the trials of each subject were averaged. Otherwise, the high dimensionality of the data would make the community detection impossible due to the computational burden.

3.2. Automatic frequency band identification

3.2.1. Recurrence plots

Recurrence plots (RP) are two-dimensional matrices that ease the detection of clusters and patterns of periodicity in the data they represent (Marwan et al., 2007; Webber and Zbilut, 2005). Originally, they were designed to detect time patterns in dynamical systems (Marwan et al., 2007). They are formulated as follows (Webber and Zbilut, 2005):

$$\mathbf{R}_{n,m}(\epsilon) = \Theta(\epsilon - \|\mathbf{X}_n - \mathbf{X}_m\|), \quad (4)$$

where \mathbf{X}_n is the time course at time n , ϵ is a threshold, $\Theta(\cdot)$ the Heaviside function, and $\|\cdot\|$ the norm. Nonetheless, in this study, we replaced the norm by the Spearman correlation between AEC matrices to avoid the selection of an arbitrary threshold (Tewarie et al., 2019b). Furthermore, as we are not working in the time domain but in the frequency domain, the RPs were defined as follows (Núñez et al., 2021; Tewarie et al., 2019b):

$$\mathbf{R}_{n,m} = \text{corr}[AEC(n), AEC(m)], \quad (5)$$

where $AEC(n)$ and $AEC(m)$ are the connectivity matrices for the frequencies n and m , respectively. Thus, the RP is used to identify frequency-dependent clusters that group connectivity matrices with a similar topological structure.

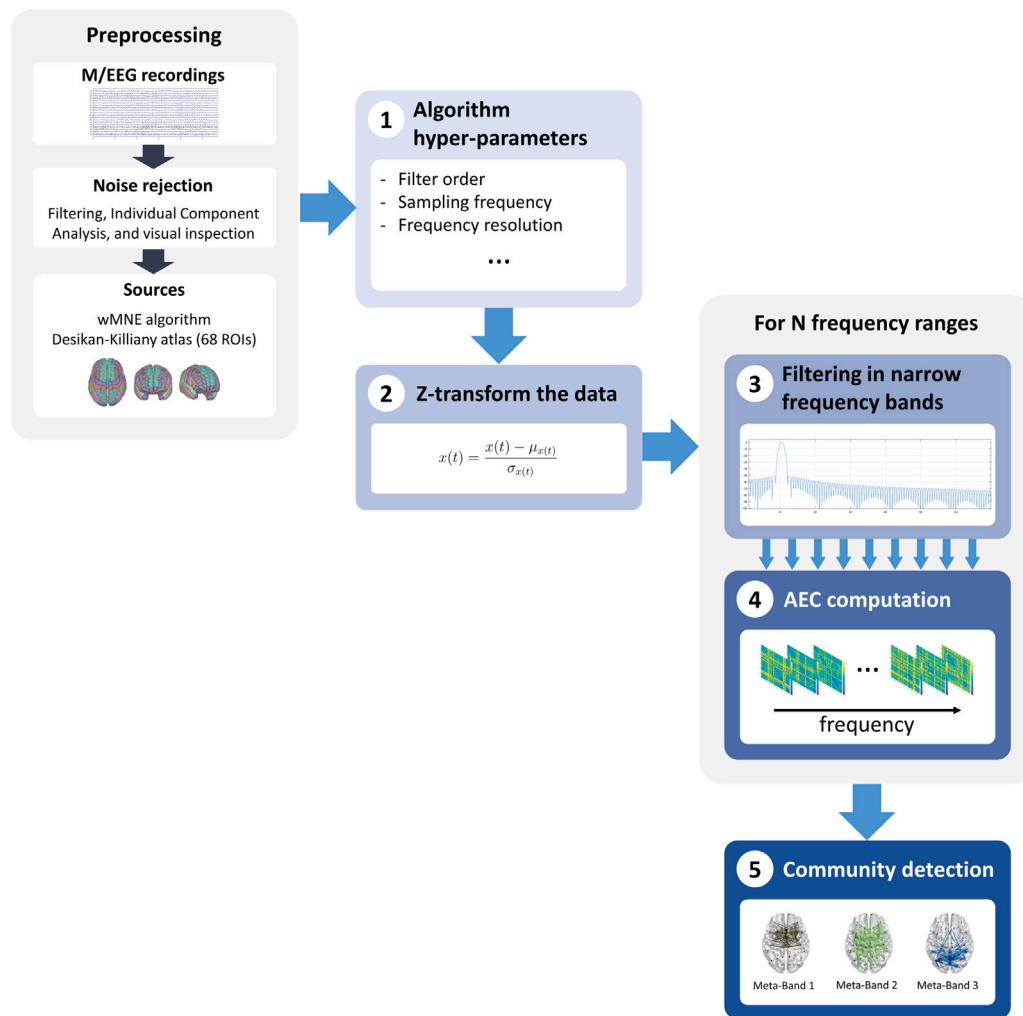


Fig. 1. Flow diagram of the study. (1) Definition of the algorithm hyper-parameters based on the characteristics of our study. (2) Normalization of the data by means of a Z-transformation. (3) Filtering of the signal in narrow (1 Hz) bands. (4) Computation of the frequency-dependent FC by means of the amplitude envelope correlation in its orthogonalized version. Steps (3) and (4) are repeated for each frequency range defined in step (1). (5) Community detection to estimate the meta-bands by means of the Louvain GJA algorithm.

3.2.2. Louvain community detection algorithm

Community detection algorithms have been used to detect clusters of brain regions (Bassett and Bullmore, 2006; Gates et al., 2016), or temporal brain meta-states (Núñez et al., 2021; Tewarie et al., 2019b; Zhou et al., 2019). Here, this methodology was used to detect repeated network patterns along the frequency dimension that can be identified as meta-bands. As we wanted to implement the frequency band identification in an unsupervised fashion, the Louvain GJA algorithm was used (Núñez et al., 2021). This method does not require the *a-priori* definition of the number of communities to discover, overcoming, in this sense, other algorithms such as *k*-means clustering, or non-negative tensor factorization (Núñez et al., 2021; O'Neill et al., 2018; Tewarie et al., 2019b; Cabral et al., 2017; Ponce-Alvarez et al., 2015).

For this task, the RP constructed in the previous section is considered as a graph, with each of the frequency-dependent connectivity matrices being the nodes, and the Spearman correlation between them being the edges. Communities were then discovered in the RP by means of the Louvain GJA method (Rubinov and Sporns, 2011; Blondel et al., 2008). The Louvain GJA method is an iterative algorithm that maximizes the modularity of its solution by assigning each node to its own community and then finding modularity maxima by moving nodes

to other communities (Gates et al., 2016). This method has been proven to perform well with poorly-defined communities (Gates et al., 2016). As the algorithm is non-deterministic, it was run 250 times, selecting the solution with highest modularity (Núñez et al., 2021).

To ease the comparison across subjects, we conducted a per-group community detection pipeline (Núñez et al., 2022). To do so, RPs were constructed by concatenating all the frequency-dependent connectivity matrices of every subject in a database (Núñez et al., 2021). Hence, community detection was carried out on square connectivity matrices with dimension N , where N is the number of subjects in a database multiplied by the number of frequency bins. The network topologies of the meta-bands were obtained by averaging all the connectivity matrices assigned to each meta-band (Núñez et al., 2021).

3.2.3. Frequency-band activation sequence (FAS), attraction strength (AS), and degree of dominance (DoD)

A metric was defined based on the community extraction performed by the Louvain GJA method, the frequency-band activation sequence (FAS). This is a symbolic function that contains the information about the dominant meta-band network topology for each frequency bin (*i.e.*, the functional connectivity configuration assigned by the Louvain

algorithm to that bin). Metrics containing information about changes between meta-states have been previously used to characterize brain state transitions (Núñez et al., 2021; Cabral et al., 2017; Baker et al., 2014). Nonetheless, the FAS only contains information regarding to which meta-band belongs each frequency-dependent connectivity matrix at each frequency bin. Consequently, in order to complement this information, two new metrics were defined: the attraction strength (AS) and the degree of dominance (DoD). These parameters measure how well the network topology of a specific frequency fits its assigned meta-band.

The AS is the Spearman correlation between each frequency-dependent connectivity matrix and the topology of the dominant meta-band (*i.e.*, the meta-band to which it has been assigned). It is calculated as follows:

$$AS(i) = \text{corr}(A_i, M_{di}) \quad (6)$$

where $\text{corr}(\cdot)$ is the Spearman correlation, M_{di} the network topology of the dominant meta-band in the frequency i , and A_i the connectivity matrix in the frequency i .

The DoD is defined as the correlation between each connectivity matrix and the dominant meta-band, minus the average correlation between that connectivity matrix and the non-dominant meta-bands. It is calculated as follows:

$$DoD(i) = \text{corr}(A_i, M_{di}) - \frac{1}{m-1} \sum_{\substack{n=1 \\ n \neq d}}^m \text{corr}(A_i, M_{ni}) \quad (7)$$

where M_{ni} is the network topology of each of the non-dominant meta-bands in the frequency i . By analysing the complementary information obtained from these metrics (FAS, AS, and DoD), we can deepen our understanding of the frequency structure of brain FC.

3.3. Assessing the algorithm performance by means of synthetic signals with known ground-truth

The performance of the CMB algorithm was evaluated with the two types of synthetic signals (amplitude-coupled and M/EEG-like). Two different types of tests were performed: (i) evaluation of the algorithm to assess whether it is able to detect meta-bands in hypothetical demanding situations; (ii) tuning of the parameters to assess their impact on the results.

In the first scenario, the following parameters were evaluated:

- **Bandwidth:** Different values of the underlying synthetic meta-band bandwidth were tested to find out whether there is a hard limit where the algorithm is unable to recover the underlying meta-band. This parameter was tested for amplitude-coupled synthetic signals.
- **Band overlap:** The presence of close frequency bands (or even overlapping ones) could also be a problem for the algorithm. This parameter was tested for amplitude-coupled synthetic signals.
- **Number of meta-bands:** This simulation was performed to assess whether the number of underlying meta-bands that the CMB algorithm is capable of recovering. This parameter was tested for M/EEG-like synthetic signals.
- **Continuous bands:** The previous test of the capability of the algorithm of recovering multiple bands was repeated again with two different band configurations. First, we considered a scenario where a frequency range with no underlying network structure was left between meta-bands. For example, if two meta-bands are defined in the range of interest between 1 and 70 Hz, they could range, *e.g.*, from 5 to 35 Hz and from 45 to 60 Hz, with a frequency band with no underlying defined network structure in between. Second, we also considered a scenario where the meta-bands were adjacent (*i.e.* the frequency range without structure that separated the meta-bands is no longer considered). That is,

if we define two meta-bands in a frequency range of interest between 1 and 70 Hz, they could range, *e.g.*, from 1 to 40 Hz and from 40 to 70 Hz. This test was carried out to assess whether the CMB algorithm is capable to detect the boundaries not only between meta-bands but also between a meta-band and a frequency region without a specific FC pattern. This parameter was tested for M/EEG-like synthetic signals.

In the second scenario, we evaluated:

- **Filter order:** The meta-bands were generated with different filter orders to assess their impact on the results. This parameter was tested for amplitude-coupled synthetic signals.
- **Sampling frequency:** Different sampling frequencies were tested to evaluate the influence of this parameter. This parameter was tested for amplitude-coupled and M/EEG-like synthetic signals.
- **Frequency resolution:** The influence of the bandwidth of the filters of the narrowband filter bank on the meta-bands was evaluated. This parameter (and the frequency range under study) define the number of frequency bins. This parameter was tested for amplitude-coupled synthetic signals.

4. Results

4.1. Assessing the CMB algorithm performance in demanding situations

The performance of the CMB algorithm in the hypothetical demanding situations defined in Section 3.3 is summarized below (a more detailed description of the results can be obtained in section 2 of the Supplementary Material):

- **Bandwidth:** The results showed wider bandwidths provide better-defined connectivity matrices, as there are more frequency bins with a given connectivity pattern. Further details are provided in section 2.1.2 of the Supplementary Material.
- **Band overlap:** The CMB algorithm is capable of detecting close, contiguous, and even overlapping meta-bands. In this latter scenario, in the frequency ranges where two meta-bands overlap, only one of them is detected. Further details are provided in section 2.1.4 of the Supplementary Material.
- **Number of meta-bands:** The CMB algorithm is able to recover any number of meta-bands. Further details are provided in section 2.2 of the Supplementary Material.
- **Continuous bands:** The CMB algorithm is able to recover adjacent and non-adjacent meta-bands. Further details are provided in sections 2.2.1 and 2.2.2 of the Supplementary Material.

4.2. Assessing the influence of the CMB algorithm hyper-parameters in the results

The results about the influence of the different hyper-parameters of the CMB algorithm in the meta-band detection can be summarized as follows (a more detailed description of the results can be obtained in section 2 of the Supplementary Material):

- **Filter order:** Lower filter orders yield a decreased frequency resolution to detect the underlying meta-band (*i.e.*, lower efficiency detecting the edges of the meta-bands). Also, higher filter orders lead to a noisier detection in the frequencies where no meta-band was specified and, thus, to less defined connectivity matrices with lower coupling values. In consequence, we have selected a filter order of 500 to get a good balance between the aforementioned effects. Further details are provided in section 2.1.1 of the Supplementary Material.

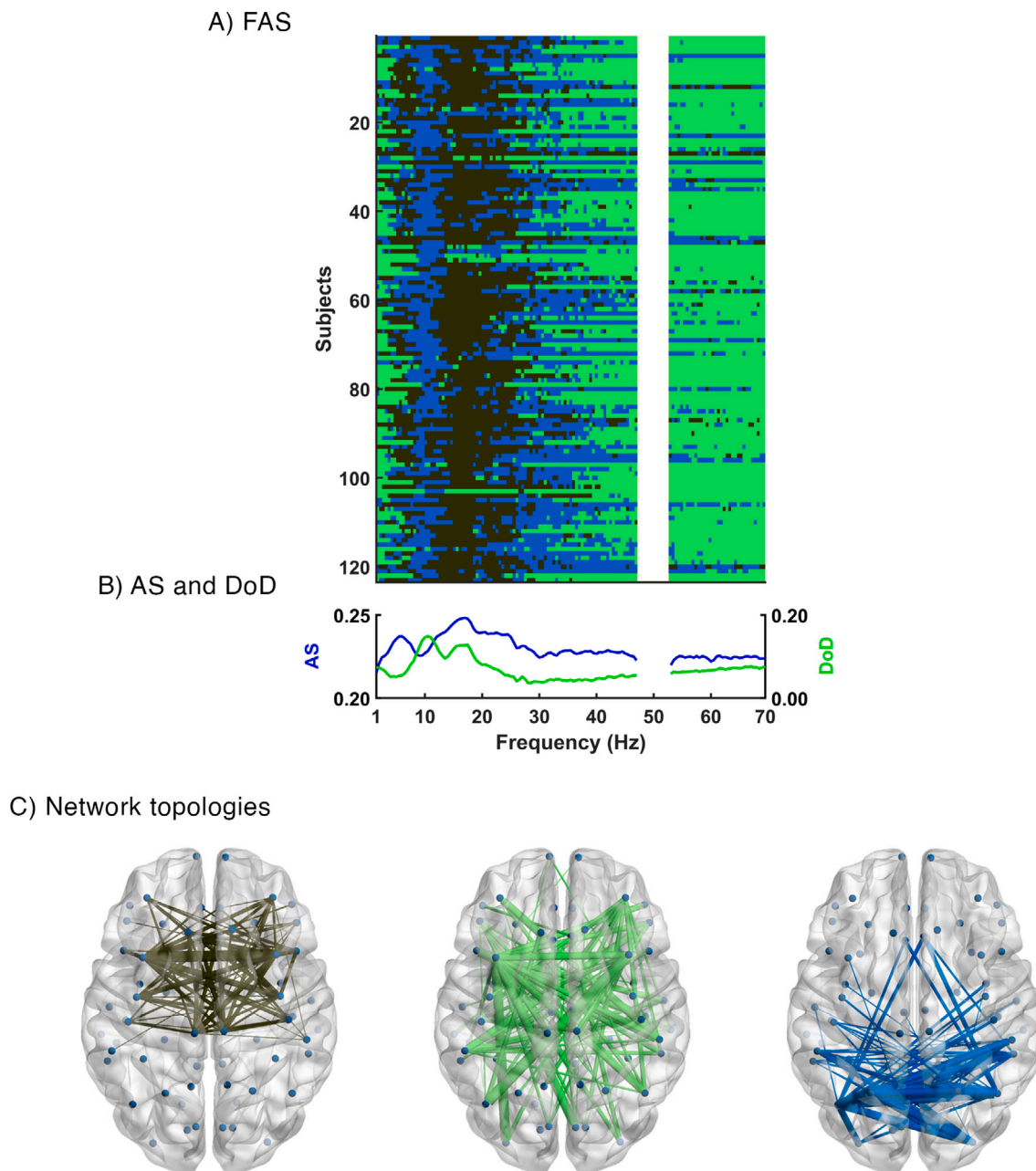


Fig. 2. Meta-bands detected with the MEG database using a filter order of 500. (A) Y-axis includes the FAS for each subject, while X-axis represents each individual frequency bin; different colours represent different communities. (B) Frequency evolution of Attraction Strength (AS, blue) and Degree of Dominance (DoD, green). (C) Network topologies of the three meta-bands detected; the colour of each network topology corresponds with the colour of the meta-bands in the upper plot. (For interpretation of the references to colour in this figure legend, the reader is referred to the web version of this article.)

- **Sampling frequency:** It can be observed that lower sampling frequencies provide slightly narrower bands for a given filter order. Besides, the lower the sampling frequency, the lower regularity in the detection (*i.e.*, spurious state changes) in frequencies where no underlying band was defined. Further details are provided in sections 2.1.3 and 2.2.3 of the Supplementary Material.
- **Frequency resolution:** Higher bandwidths of the narrowband filter bank are associated with decreased frequency resolution in the results. Of note, increasing the frequency resolution increments the computational burden of the CMB algorithm. Further details are provided in section 2.1.5 of the Supplementary Material.

4.3. Assessing the CMB algorithm with real signals

The assessments carried out with synthetic signals helped us to decide which parameters to select when computing the CMB algorithm in real signals. First, the original sampling frequency was used for the three databases. The bandwidth of the filters was set to 1 Hz (thus being the CMB algorithm capable to detect 1 Hz bands), as lower values will dramatically increase the computational burden. As previously indicated, higher values of this factor will provoke solutions with lower frequency resolution, and less spurious meta-band transitions. This can be appreciated in Figures S20 and S21 in Supplementary Material.

All the analyses were conducted between 1 and 70 Hz. Of note, the connectivity matrices around 50 Hz (47.5–52.5 Hz) were discarded as they are highly influenced by the 50 Hz power-line artefact (and its associated notch filtering process) (Rodríguez-González et al., 2021). In line with the findings observed in the synthetic signals, a filter order of 500 was employed. To ensure convergence of the Louvain GJA algorithm, the number of iterations was set to 250, although 100 iterations have been proven to be enough (Núñez et al., 2021). It is noteworthy that the specific values of these parameters can be adapted to fit the requirements of each study.

Fig. 2 summarizes the meta-bands detected for the MEG database. The corresponding AS and DoD values are also depicted, as well as the topology for the three meta-bands networks detected. A fronto-medial network meta-band (brown) that is dominating approximately from 15 to 25 Hz can be observed. In addition, there is a medial network meta-band (green) that is mainly dominating in low (1–5 Hz) and high (35–70 Hz) frequencies. Finally, there is a parieto-occipital network meta-band (blue) that dominates around alpha (5–15 Hz) and beta-2 bands (25–35 Hz). Regarding the AS, it could be observed that it decreases in: (i) the low frequencies; (ii) the blue meta-band around alpha; and (iii) from 30 Hz on. The higher AS values, the better the adjustment of individual frequency-dependent connectivity matrices with the corresponding meta-band network topology. Moreover, it can be appreciated that the DoD has two peaks: (i) in the blue meta-band around alpha; and (ii) in the brown meta-band. An increase of this value indicates a higher topological distance between the dominant meta-band and other meta-bands.

Fig. 3 shows the meta-bands as well as their corresponding AS, DoD, and topologies for the EEG₁ database. The differences with the meta-bands features detected for the MEG database are noteworthy, nonetheless, it can also be observed some similarities. There is a meta-band dominating from 1 Hz to approximately 30 Hz (brown) and another meta-band dominating from 30 to 70 Hz (green). Moreover, the blue meta-band only appears in some subjects from 20 Hz on, and in a few isolated frequencies. In addition, the brown meta-band displays a parieto-occipital topology similar to the blue meta-band of the MEG database. The green meta-band displays a fronto-medial topology, and the blue one a right-medial network configuration. Finally, AS and DoD parameters show a peak around 10 Hz: while the peak of the AS is negative, the peak of the DoD is positive (similar to the behaviour of DoD in the MEG database).

Fig. 4 summarizes the meta-bands as well as their corresponding AS, DoD, and topologies for the EEG₂ database. The frequency distribution of the meta-bands is very similar to the one of the EEG₁: the brown meta-band dominates approximately from 1 to 30 Hz; the green meta-band dominates approximately from 30 to 70 Hz; and the blue meta-band only appears in some subjects from 20 Hz on, and in a few isolated frequencies. Furthermore, the topologies of the green (fronto-medial) and blue (right-medial) meta-bands are also similar to those found in the EEG₁ database. On the other hand, the network configuration of the brown meta-band is different from that for the EEG₁ database, having a medial topology. Both AS and DoD present a negative peak around 10 Hz, with a steeper decline for the AS.

The results in Figs. 2, 3, and 4, but calculated with a filter order of 1500, are also included in Supplementary Material in Figures S22 (MEG database), S23 (EEG₁ database), and S24 (EEG₂ database). There, the noisier meta-band detection obtained when using 1500 as filter order can be appreciated. The problem of noisy detection was also observed in previous studies (Núñez et al., 2021, 2022).

In addition, the extent to which the CMB algorithm fits other approaches used to automatically define the frequency bands was assessed for MEG signals. To do that, we quantified the alignment of the meta-band in the alpha range (blue meta-band) with other definitions of this frequency band, as it is known that alpha band plays an important role in resting-state recordings (Bazanov, 2012). Two definitions to estimate the alpha band were evaluated: the canonical

alpha band (8–13 Hz), and an adaptive alpha band based on estimating the individual alpha frequency (IAF) and considering the alpha band as: $IAF \pm 2$ Hz. (Vecchiato et al., 2011; Babiloni et al., 2010). This process was only performed for the MEG database, as the EEG databases lack a clear meta-band specific to the alpha frequencies. In Fig. 5 the overlap of the detected meta-bands with the canonical (A) and adaptive (B) alpha band approaches is depicted. For the canonical approach, our alpha meta-band is present in a 59.7% of the frequency bins, while for the adaptive approach the degree of overlap of our alpha meta-band is 67.4%. In addition, in Fig. 6 the modal meta-band across subjects is depicted, showing a remarkable consistency with the canonical definition of the frequency bands (shown in a bar above): delta: 1–4 Hz, theta: 4–8 Hz, alpha: 8–13 Hz, beta: 13–30 Hz, and gamma: 30–70 Hz. Besides, in that Figure the network topologies of both, the canonical bands and the meta-bands are also displayed. These network topologies support the validity of the results obtained by the CMB algorithm, as there is a remarkable coincidence between the network topology of the meta-bands and the topology of canonical bands in the frequencies where they are present: brown meta-band presents a connectivity pattern similar to those for delta and gamma bands; the network topology of the green meta-band is similar to those of theta, beta-1, and beta-2; and blue meta-band has a connectivity pattern similar to that of alpha.

5. Discussion

In this study, we introduced a new method to study the frequency structure of the functional connectivity in resting-state signals. We performed a community detection procedure along the frequency dimension to unveil the underlying meta-bands, which were grouped according to the similarity of their network topology. Our findings showed that: (i) the CMB algorithm is sensitive to individual idiosyncrasies at subject level, providing a new framework to further understand the frequency structure of functional brain networks; (ii) this frequency structure is dominated by a limited number of meta-bands (*i.e.*, connectivity topologies), that possibly play different roles depending on the frequency range; and (iii) MEG is more sensitive than EEG to characterize the underlying frequency structure of functional connectivity.

5.1. Revisiting canonical frequency bands

The well-known canonical frequency bands are supported by a large body of studies. It is clear that they reflect underlying physiological mechanisms (Sanei and Chambers, 2021; Buzsáki and Draguhn, 2004). Nonetheless, there are a variety of issues related with their definition that lead us to look for an automatic, unsupervised, and adaptive frequency segmentation in connectivity studies. The first issue is that they were defined about 80 years ago, using the rudimentary EEG systems that were available at the time (Jasper and Andrews, 1936; Berger, 1934; Walter and Dovey, 1944). Since then, technology and, as a consequence, recording systems have dramatically changed, and are now able to record neural activity with a highly increased quality. Because of this, it is reasonable to hypothesize that nowadays more accurate frequency bands segmentations can be performed. The next issue is related with the frequency bands limits. The literature shows a great inconsistency in the definition of the specific limits of the canonical frequency bands (Newson and Thiagarajan, 2019). Thus, even though the name of the bands is preserved, their specific definition varies across studies (Newson and Thiagarajan, 2019). The third issue is that analysis methods have deeply evolved since the original definition of the canonical frequency bands. The current analysis techniques are able to measure different patterns of neural activity than the ones used to define the canonical bands. For example, functional connectivity reflects global (and local) neural synchronization, while the methods

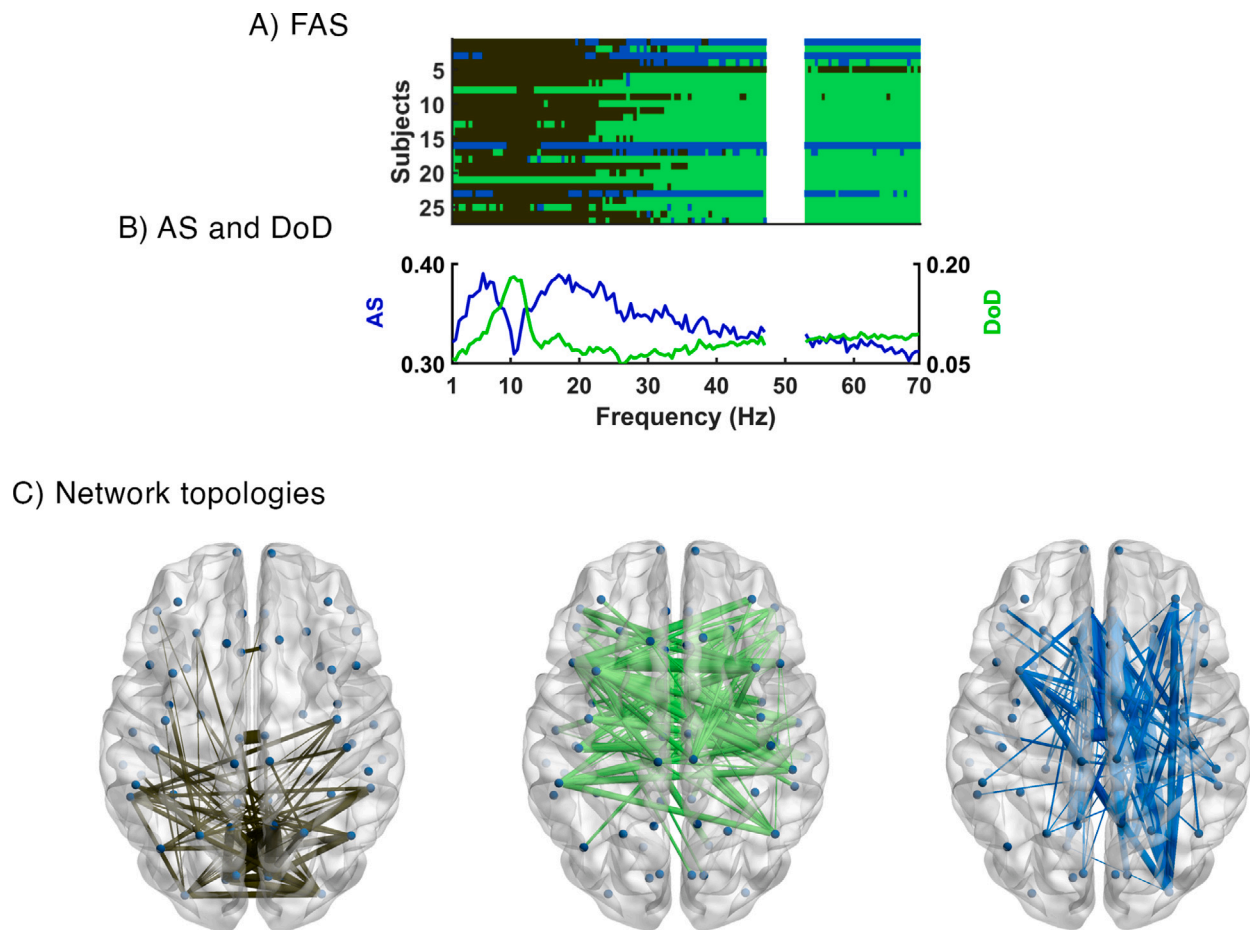


Fig. 3. Meta-bands detected with the EEG₁ database using a filter order of 500. (A) Y-axis includes the FAS for each subject, while X-axis represents each individual frequency bin; different colours represent different communities. (B) Frequency evolution of Attraction Strength (AS, blue) and Degree of Dominance (DoD, green). (C) Network topologies of the three meta-bands detected; the colour of each network topology corresponds with the colour of the meta-bands in the upper plot. (For interpretation of the references to colour in this figure legend, the reader is referred to the web version of this article.)

used to define the canonical bands only reflect local neural synchronization (Stam and van Straaten, 2012; Rodríguez-González et al., 2021; Tewarie et al., 2019a). Finally, the canonical frequency bands do not account for the individual idiosyncrasies, *i.e.*, the differentiating brain patterns across individuals. In line with this, there is an increased interest in personalized analyses, which have led to the definition of adaptive frequency bands (Pascarelli et al., 2020; Borghini et al., 2019). Our methodology allows to define user-specific frequency bands, with a data-driven method that permits an increased level of personalization regarding the currently used adaptive approaches.

It has to be indicated that a direct comparison between the CMB algorithm and the canonical bands is not possible. The CMB algorithm disregards all the assumptions made by the canonical bands and, hence, the resulting frequency segmentation is so different that the direct comparison with the canonical bands is not possible: the frequency ranges are different, the number of meta-bands does not match, and the meta-bands expand across non-adjacent frequency ranges. Additionally, although the topologies of the canonical frequency bands showed a remarkable coincidence with their (approximate) corresponding meta-bands, this analysis is too simple to make direct associations between meta-bands and canonical bands. Furthermore, the limits of the canonical bands are not clear, as there is a great inconsistency in their definition (Newson and Thiagarajan, 2019). Consequently, we decided to only compare the alpha band of these previous approaches with the meta-band associated with alpha (the blue meta-band) in the MEG database, as it has been observed that alpha activity dominates neural dynamics during eyes-closed rest condition (Millett, 2001; Trajkovic

et al., 2021). It can be appreciated that our blue meta-band has an occipital connectivity pattern, similar to that observed in the canonical alpha band. Of note, the adaptive alpha band showed higher coincidence (67%) with our alpha meta-band compared to the canonical alpha band (60%). This suggests that, although the traditional band segmentation approaches provide a good starting point for fitting the underlying topological structure at group-level, the individual idiosyncrasies are not fully accounted for. In this regard, the CMB algorithm is useful as it automatically adapts to the specific neural patterns of each subject, with no *a-priori* assumptions, as the canonical and adaptive approaches do.

The majority of the currently available user-specific band segmentation approaches are based on detecting spectral peaks, which can be problematic in the absence of observable peaks in the power spectral density (Cohen, 2021). In consequence, it is difficult to compare our meta-bands with previous studies as, to the best of our knowledge, only two previous works have assessed the frequency structure of functional connectivity (Cohen, 2021; Puxeddu et al., 2021). The study conducted by Puxeddu and colleagues (Puxeddu et al., 2021) employed a community-detection algorithm in frequency-specific connectivity matrices. Nonetheless, the research was not aimed at proposing an alternative frequency segmentation method, but to use a multi-layer model to analyse multi-frequency EEG networks (Puxeddu et al., 2021). On the other hand, based on the idea that the current band segmentation approaches add uncertainty and subjectivity to the analyses, Cohen (Cohen, 2021) proposed an alternative band segmentation approach. He used covariance matrices to identify patterns that

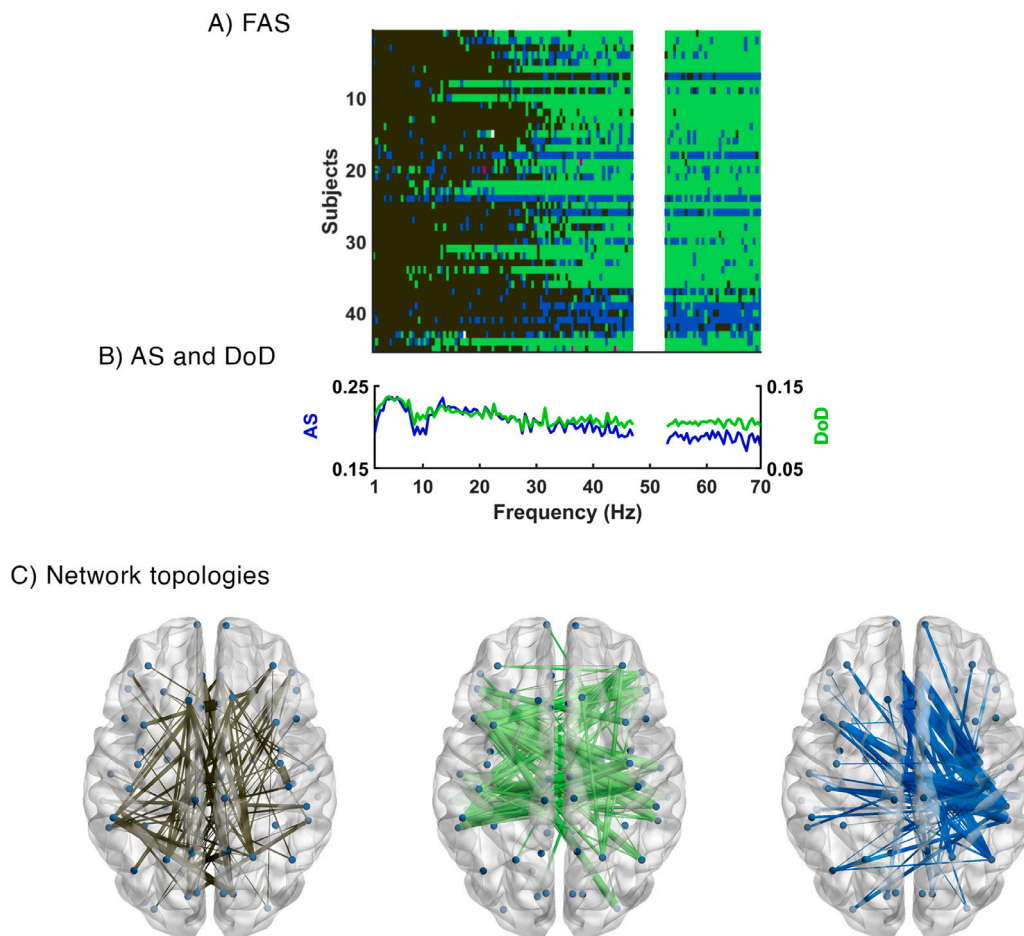


Fig. 4. Meta-bands detected with the EEG₂ database using a filter order of 500. (A) Y-axis includes the FAS for each subject, while X-axis represents each individual frequency bin; different colours represent different communities. (B) Frequency evolution of Attraction Strength (AS, blue) and Degree of Dominance (DoD, green). (C) Network topologies of the three meta-bands detected; the colour of each network topology corresponds with the colour of the meta-bands in the upper plot. (For interpretation of the references to colour in this figure legend, the reader is referred to the web version of this article.)

maximally separate the spatio-temporal narrowband activity from the spatio-temporal broadband activity. Then, he grouped these patterns using the *dbscan* clustering algorithm, resulting in its user-specific bands (Cohen, 2021). His results showed a great variability across subjects in the number of detected frequency bands (ranging from 4 to 11), and also in the limits of the personalized alpha band (with the lower bound ranging approximately from 3 to 10 Hz, and the upper bound ranging approximately from 6 to 18 Hz). Our results support the heterogeneity in band segmentation found in this previous work, which suggests the need for individualized analyses that accounts for these user-specific idiosyncrasies. The CMB algorithm performs an individualized band segmentation derived from the connectivity-based spatio-frequency patterns obtained by means of the AEC method, as it is robust and repeatable (Colclough et al., 2016; Schoonhoven et al., 2022). In addition, the CMB algorithm uses the Louvain GJA algorithm, as it does not *a-priori* define any parameter to achieve a satisfactory performance (Núñez et al., 2021, 2022). In consequence, to the best of our knowledge, this is the first study that proposes a subject-specific frequency band segmentation based on the topological properties of the frequency-dependent connectivity matrices.

All these findings led us to define some general ideas on the use of the “canonical” frequency bands. On the one hand, their use when working with resting-state EEG signals in connectivity analyses should be carefully considered. Our results indicate that the use of these bands can introduce a significant bias, as their parcellation of the frequency range does not reflect the underlying frequential structure of functional connectivity. In this regard, the CMB algorithm could be a better

alternative as it fully adapts to the frequency-dependent connectivity patterns. On the other hand, the scenario for MEG resting-state connectivity analyses is more complicated to analyse. The “canonical” frequency bands are convenient, as they provide a common framework that eases the comparison across studies; however, their definition is not consistent (Newson and Thiagarajan, 2019), and they do not take into account subject-specific neural traits. In this regard, we consider that, while “canonical” frequency bands can be an acceptable proxy of the underlying frequency-dependent network structure, they are missing the individual particularities that should be accounted to obtain accurate results, as well as a better understanding and more meaningful interpretations of the phenomena under study. In summary, we think that, whenever the computational capabilities make it possible, the CMB algorithm should be employed in resting-state MEG connectivity studies. Nonetheless, it could be also convenient to complement those analyses with the conventional segmentation into “canonical” frequency bands, to facilitate a more straightforward comparisons with previous studies.

5.2. Unveiling the fundamental functional network configurations

Regarding the number of meta-bands detected for the different databases, a relevant conclusion can be drawn. Whereas in the MEG signals 3 clearly defined communities are observed, in the EEG databases only 2 dominant communities are detected, being the third one only present in isolated frequency bins and subjects. Of note, these results do

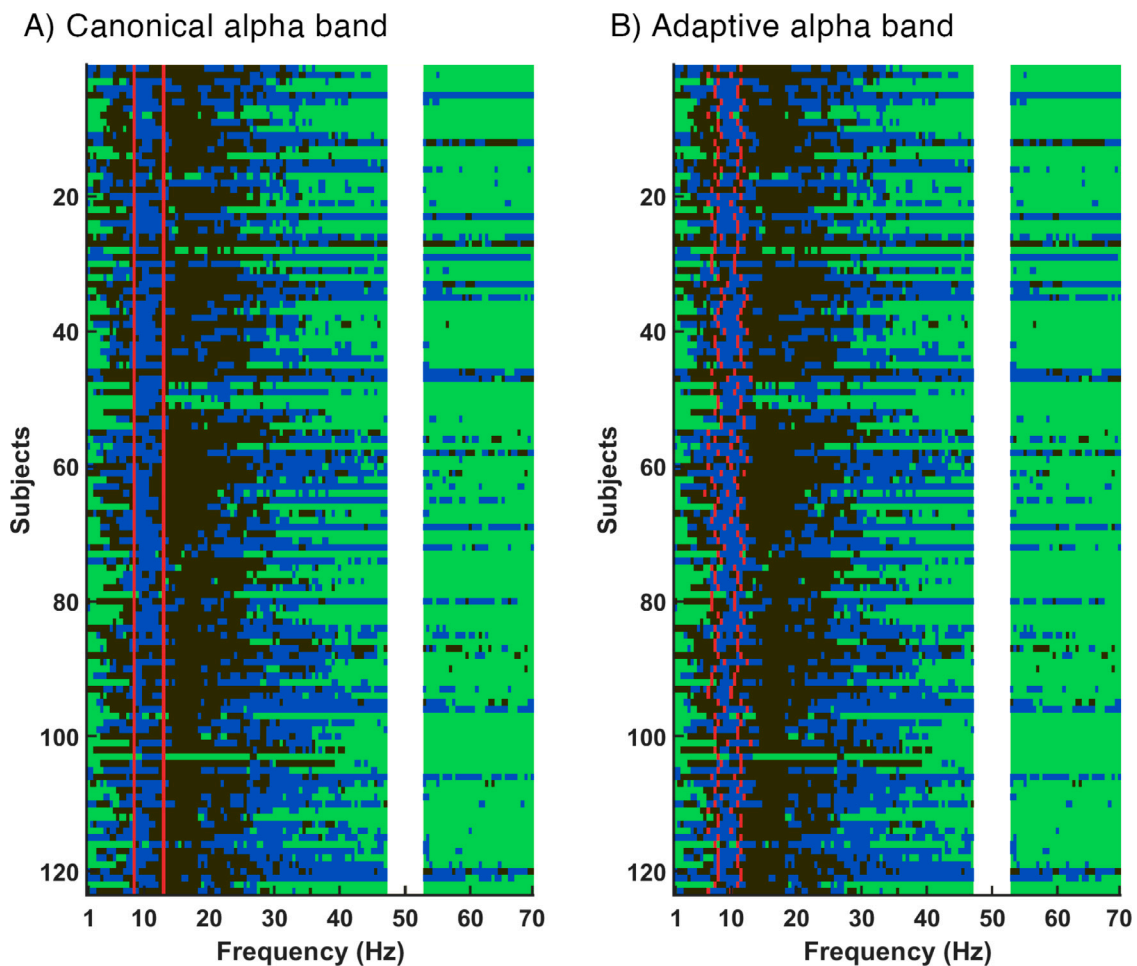


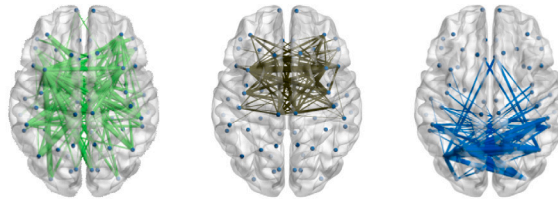
Fig. 5. Overlapping of meta-bands (for the MEG database using a filter order of 500) with other alpha band definitions: (A) canonical alpha band (8–13 Hz); (B) adaptive alpha band (individual alpha frequency \pm 2 Hz). The alternatives definitions of the alpha band are delimited with two red lines. The Y-axis includes the FAS for each subject, while the X-axis represents each individual frequency bin; different colours mean different communities. (For interpretation of the references to colour in this figure legend, the reader is referred to the web version of this article.)

not mean that our resting-state neural activity displays only 2 or 3 specific network topologies; they mean that there are 3 network topologies that recurrently appear across frequencies during the resting-state.

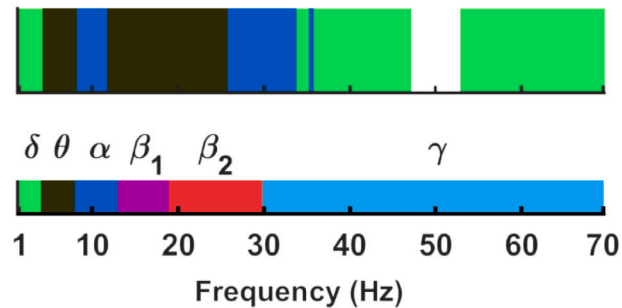
As this is the first study that extracts frequency meta-bands, it is not easy to find previous researches to which to relate the results. However, it may be interesting to consider our meta-bands as the frequential counterparts of the brain meta-states extracted on dynamic functional connectivity (dFC) analyses. The so-called brain meta-states are network patterns that are recurrently repeated over time, considering that the connectivity matrix in each time sample is a weighted combination of the identified meta-states (Zhao et al., 2019; Mennigen et al., 2018). In this regard, the number of recurrent network topologies detected in the MEG database (*i.e.*, 3) is in agreement with a previous study, where 3 time-recurrent network topologies were extracted in resting-state EEG signals from healthy elderly subjects (Núñez et al., 2021). Although in the literature, different number of meta-states have been identified, its repertory is usually limited, considered to follow a heavy-tail distribution, with a few meta-states being activated very frequently (von Schwandenflug et al., 2023). This is consider to provide a cost-efficient modular way of processing neural information (von Schwandenflug et al., 2023; Ramirez-Mahaluf et al., 2020). Thus, it is reasonable to hypothesize that the limited number of meta-band topologies that we have identified may also be a consequence of the optimization of neural information processing. In line with that, it has been proposed that one of the main variables ruling out brain organization may be economical constraints (Bullmore and Sporns, 2012).

Another interesting finding is that the meta-bands are distributed across disjointed frequency ranges: for the MEG database, the green meta-band is present around the canonical delta and gamma bands, and the blue meta-band is present around canonical alpha and beta-2 bands. This contradiction could be explained by three factors. First, this can be due to a mixing effect provoked by averaging different trials from resting-state activity, which has been found to exhibit a highly dynamic repertoire of recurrent network topologies (Núñez et al., 2021). Second, it could be due to cross-frequency coupling. Several studies have addressed the potential relationships between different frequency bands, observing that these interactions play an important role in the processing and transmission of neural information (Händel and Haarmeier, 2009; Cho et al., 2015; Riddle et al., 2021). Particularly, cross-frequency patterns have been demonstrated to play an important role in resting-state activity, as they contribute to long-range communication (Florin and Baillet, 2015; Stankovski et al., 2017). In this regard, previous studies on this field have observed interactions between slow-frequency (delta and theta) and high-frequency (beta and gamma) oscillations (Händel and Haarmeier, 2009; Cho et al., 2015; Riddle et al., 2021), which could shape the functional network patterns at these frequency ranges. Finally, this distant coupling can be due to the fact that we are grouping frequency bands based on their underlying network topology. Hence, this does not necessarily indicate there are only 2 or 3 global meta-bands, but similar network topologies operating across different frequencies (Uhlhaas et al., 2008). In this regard, it can be hypothesized that this is the result of the brain optimizing

A) Network topologies of the meta-bands



B) Comparison of meta-bands and canonical frequency bands



C) Network topologies of the canonical frequency bands

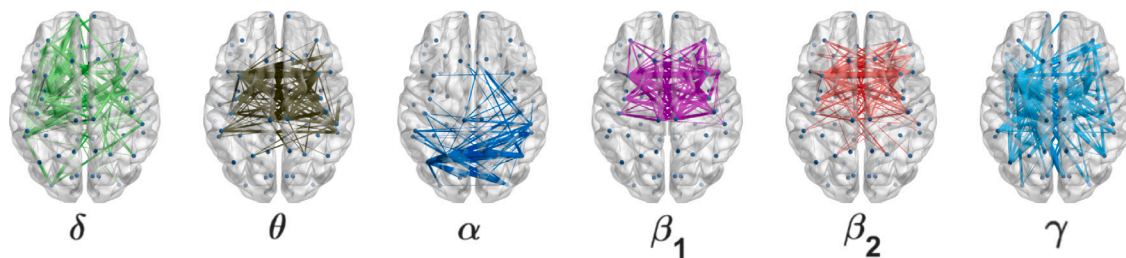


Fig. 6. Comparison of meta-bands (for the MEG database using a filter order of 500) with canonical frequency bands. (A) Network topologies of the identified meta-bands. (B) In the upper part, the mode of the meta-bands across all the subjects is depicted, below there is a bar showing the canonical definition of the frequency bands (δ : 1–4 Hz; θ : 4–8 Hz; α : 8–13 Hz; β_1 : 13–19 Hz; β_2 : 19–30 Hz; and γ : 30–70 Hz). (C) Network topologies of the canonical frequency bands. Different colours represent different communities. (For interpretation of the references to colour in this figure legend, the reader is referred to the web version of this article.)

resources (Bullmore and Sporns, 2012), having a reduced number of topologies integrating different functions depending on the frequency range they are operating (Uhlhaas et al., 2008). It has been suggested that the brain has timescale-dependent network organizations (Sasai et al., 2014; Bola and Sabel, 2015). Our results extend that hypothesis indicating that some of those topologies could be repeated (at least to some extent) across frequencies. This is supported by previous studies that revealed that some graph characteristics of neural networks were preserved across frequencies (Bullmore and Sporns, 2009; Bassett et al., 2006). Besides, this can be observed in Fig. 6 that compares meta-bands and canonical frequency bands in both, sequencing, and topology. This Figure shows that, although there are some bands historically considered different, from a mathematical perspective and based on the underlying network topology, they could be considered as closely related.

The blue MEG meta-band, which we have associated with the canonical alpha band, presents a parieto-occipital topology. This meta-band does not fit its corresponding frequency-dependent connectivity matrices very well; however, it does it remarkably better than the other (*i.e.*, non-dominant) meta-bands. A similar topology can be appreciated for the EEG₁ database in its brown meta-band, which is the meta-band present around the canonical alpha band. On the other hand, the brown meta-band from EEG₂, which is again present in the frequencies

around the canonical alpha band, depicts a medial widespread topology. Around this meta-band, DoD and AS values decrease, indicating that the brown meta-band is not fitting the underlying network topology properly. This suggests that the increased sampling frequency and spatial resolution of the EEG₁ database have improved the sensitivity of the signals to reflect the underlying network structure, although still not to the same extent as in MEG signals. The network topology of this meta-band is similar to that observed in other studies, which found parieto-occipital networks for resting-state M/EEG signals in the alpha band (Colclough et al., 2016; Miraglia et al., 2017; Hillebrand et al., 2012). This occipital topology could be related to the posterior areas of the default-mode network (DMN), which has been proposed to be the dominant brain activity during rest. Some studies have suggested that the DMN consist of two subnetworks: anterior DMN, and posterior DMN (Raichle and Snyder, 2007; Raichle et al., 2001; Fauchon et al., 2022; Vidaurre et al., 2018). This association with the posterior DMN is supported by previous studies which found that these areas were strongly active (Fauchon et al., 2022; Vidaurre et al., 2018), and highly connected (Vidaurre et al., 2018) in the alpha frequencies during rest. Interestingly, the posterior areas of the DMN have been associated with higher cognitive functions such as the integration of information, attention, empathy, self-consciousness mental thoughts that occur during rest, and theory of mind (Culham and Kanwisher, 2001; Raichle and Snyder, 2007; Fauchon et al., 2022).

The brown meta-band of the MEG signals has a fronto-central topology. Its high AS and DoD values suggests that this meta-band appropriately fits its corresponding frequency-dependent matrices, even remarkably better than the other meta-bands. A similar beta-band network topology has been observed in a previous study using MEG resting-state recordings (Hillebrand et al., 2012). Although this association is not as clear as for the blue meta-band, this topology could be associated with the anterior areas of the DMN (Fauchon et al., 2022; Vidaurre et al., 2018). This network has been observed to be highly active for low frequencies (around theta), but not in beta (Fauchon et al., 2022; Vidaurre et al., 2018). The anterior areas of the DMN are involved in high cognitive functions such as semantic integration, emotions, and decision making (Tsapkini et al., 2011; Fellows and Farah, 2007). The beta frequency activation of this meta-band may be related with the sensorimotor network, which has been reported to be very active and connected around beta frequencies, and displays a topology with some areas overlapping with the brown meta-band (Fauchon et al., 2022). This network is also highly reported in intrinsic neural activity, and is involved in perception, proprioception, and motion (Chenji et al., 2016; Feher, 2012; Caspers et al., 2021). On the other hand, the beta band has also been reported to assume a critical function in the formation of canonical resting-state networks (Hipp et al., 2012), which implies a relevant role in the processing of information within and across cortical circuits (Little et al., 2019), and may explain the role of brown meta-band.

It is worth mentioning that all these brain topologies were identified using the orthogonalized version of the AEC. The orthogonalization process removes the zero-lag connectivity, as it is considered to be the result of spatial leakage leading to spurious connections (Brookes et al., 2012; Colclough et al., 2016). However, it has been proven that zero-lag couplings contain relevant information regarding the transmission of information, specially between homotopic neural areas (O'Reilly and Elsabbagh, 2021). Notably, different explanations were given to these couplings. For example, antiphase coupling is attributed to interhemispheric inhibition dynamics (O'Reilly and Elsabbagh, 2021; Perez and Cohen, 2009). Additionally, in-phase synchrony could also be explained by subcortical drivers projecting to different brain areas (Huang and Pipa, 2007), or by cortico-cortical or cortico-thalamocortical projections (Uhlhaas et al., 2009; Vicente et al., 2008). It has been also suggested that this zero-lag connectivity can be involved in the predictive capacity of the brain (O'Reilly and Elsabbagh, 2021). Different methods have been proposed to evaluate FC while avoiding leakage effects without disregarding these relevant zero-lags couplings (Farahibozorg et al., 2018; Hauk et al., 2022). However, differentiating genuine zero-lag interactions from spurious ones is still an open issue (O'Reilly and Elsabbagh, 2021). In this regard, in line with the literature (Bastos and Schoffelen, 2016; Brookes et al., 2012; Colclough et al., 2016; Khadem and Hossein-Zadeh, 2014; Schoffelen and Gross, 2009; Stam et al., 2007), we consider that the spurious zero-lag couplings could be biasing our CMB algorithm and, therefore, we decided to discard all of them by using the PLI as the connectivity measure. Nevertheless, it is important to consider that, while our frequency-dependent connectivity patterns reflect most of the functional interactions between brain regions, there are subtle aspects of these interactions that may be lost.

5.3. Differences in the underlying connectivity patterns between EEG and MEG

Of note, it was observed that a similar wide-sense frequency structure is detected in MEG and EEG. However, the results obtained from the EEG databases are missing a specific meta-band around the canonical alpha band that the CMB algorithm is able to recover in the MEG database. There are several differences between the MEG and EEG datasets that could explain the decreased EEG sensitivity to the underlying frequency structure: reduced signal-to-noise ratio (Fred et al., 2022;

Illman et al., 2020), decreased robustness against volume conduction effects (Rampp and Stefan, 2007), reduced sampling frequency, lower number of sensors, or reduced sample size, among others. To assess the latter factor, we performed an additional test by re-calculating the meta-bands detected for the MEG database but only including in the analysis 27 random subjects (as in the EEG₁ database). The results are shown in supplementary Figure S25. By doing this, the meta-band detection only slightly changed, with the blue meta-band still clearly detected around the canonical alpha band. In the second test, the influence of the number of sensors was evaluated. To this end, we constructed two new data subsets using the MEG recordings, matching in the number of sensors and sample size of the EEG₁ and EEG₂ databases. As a result, we obtained two new MEG subsets: (i) one with 32 sensors and 27 subjects, and (ii) other with 19 sensors and 45 subjects. The results are displayed in supplementary Figure S26. It can be appreciated that the detection of the three meta-bands is maintained, although there are some differences that can be due to two factors: (i) the reduced sample size (as previously described); and (ii) the reduced number of sensors. The influence of the sampling frequency was already assessed as a potential confounding factor in the CMB algorithm. It was observed that for the M/EEG-like synthetic signals, this parameter moderately affected the meta-band detection. This was also analysed with real signals by downsampling the MEG database to 200 Hz (as in the EEG₂ database) and estimating the meta-bands again. The results are shown in supplementary Figure S27 and indicate that the meta-band detection has changed, though the blue meta-band is still clearly detected in the frequencies around the canonical alpha band. However, its presence is less evident than for 1000 Hz. Thus, our findings suggest that the sampling frequency could be, at least partially, influencing the results of the EEG databases. To sum up, these results indicate that these factors (i.e., spatial resolution and sampling frequency) are not sufficient to explain the differences observed between EEG and MEG datasets. In line with this, it can be appreciated that the meta-band detection in the EEG₁ database is similar to that obtained in the EEG₂ database, despite the remarkable differences in their spatial resolution (32 vs. 19 channels) and sampling frequency (500 vs. 200 Hz). Thus, we can conclude that the discrepancies between EEG and MEG are due to the intrinsic dissimilarities between both techniques (Babiloni et al., 2009; Rampp and Stefan, 2007; Lopes, 2013; Ahlfors et al., 2010), suggesting an increased sensitivity of MEG to reflect the underlying frequency-dependent network structure.

5.4. Limitations and future lines

Although this study yielded interesting and promising results, introducing a new methodology to carry out analyses of the frequential structure of functional brain connectivity, it has some limitations that deserve further discussion.

First of all, we observed a divergence in the results between the MEG and EEG databases. Although several possible reasons to explain the differences have already been discussed, further research is required to find whether it is possible to design a methodology capable of detecting similar meta-bands for EEG signals as those in the MEG database. In line with that, it would also be interesting to evaluate other EEG datasets (with different number of channels and sampling frequencies) using the methodology proposed in this paper. Additionally, different source localization algorithms could be employed to find the extent to which the source inversion method influences the band segmentation achieved by the proposed methodology.

Furthermore, although the introduced methodology is based on a data-driven, automatic algorithm, there are some parameters that could be optimized to adapt specific user requirements (i.e., frequency resolution of the filters, filter order, or sampling frequency, among others). It is likely that the most important parameter is the filter order, with higher values of this parameter providing frequency-accurate solutions

(but with an increased presence of noise) and lower values providing smoother solutions.

Moreover, future work should upgrade the implementation of the CMB algorithm to address some of its limitations. In this regard, an interesting new feature would be allowing to configure whether the CMB algorithm accepts meta-bands covering non-adjacent frequency ranges or not. Of note, the implementation of this feature would require prior efforts addressing the issue of spurious meta-band changes (*i.e.*, changes that occur only for isolated frequency bins). Also, the application of the CMB algorithm is now based on the orthogonalized AEC. It has been observed that different connectivity metrics may reflect different neural mechanisms (He et al., 2019; Schoonhoven et al., 2022); thereby, in the future, the CMB algorithm could also include new connectivity metrics such as robust phase-based metrics. Moreover, the applied orthogonalization process is removing zero-lag associations that are sometimes considered spurious due to leakage effects (Colclough et al., 2016); however, they can also contain relevant information (O'Reilly and Elsabbagh, 2021). Hence, in future analyses, it could be interesting to explore approaches that do not remove this connectivity (Farahibozorg et al., 2018; Hauk et al., 2022). Additionally, we have based the meta-band segmentation only in the FC patterns. Although these dynamics also reflect, to some extent, information about the oscillatory amplitude, the implementation of the CMB algorithm should be extended to support other input data sources to perform the community detection (Rodríguez-González et al., 2021; Tewarie et al., 2019a; Demuru et al., 2020), as power topologies or hybrid data merging FC and power topology information. Furthermore, the CMB algorithm was developed considering the functional connectivity stable across time. This was done due to the high computational cost and complexity associated with considering its dynamic behaviour (dFC approach); nonetheless, in future studies, the CMB algorithm could be updated to support also dFC analyses. Besides, it would also be interesting to merge our methodology with the one previously proposed by Núñez and colleagues, combining time meta-states and frequency meta-bands to provide the time–frequency “building-blocks” of neural dynamics (Núñez et al., 2021, 2022).

Finally, the study was conducted with resting-state signals. Further task-related studies should be carried out to assess the potential of the introduced methodology to analyse the changes in the frequential structure of functional brain networks during an structured task. To this end, it could be interesting to determine the time intervals where the phenomenon of interest occurs, and then identify the corresponding meta-bands. This approach has the potential to enhance our comprehension of how the brain responds to specific stimuli or which neural substrates enable different cognitive processes by providing a more accurate and specific evaluation of M/EEG activity. In this regard, it could be specially interesting to combine the CMB algorithm with the methodology developed in Núñez et al. (2022), as it would allow to disentangle how these meta-bands patterns change over time.

6. Conclusions

In this study, we propose a novel frequency band segmentation approach based on the topology of the functional connectivity matrices in narrow frequency ranges. The data-driven, automatic frequency band segmentation proposed here presents a remarkable coincidence with the “canonical” frequency bands at group level, but it demonstrates this frequency parcellation ignores individual idiosyncrasies that may be biasing previous studies. Interestingly, we have also observed that the sensitivity of EEG signals to frequency-dependent connectivity neural patterns is not sufficient to identify an underlying structure aligned with the “canonical” frequency bands.

This study opens the way for personalized, data-driven connectivity analyses, allowing an objective definition of frequency ranges of interest based on the topological similarity of the functional brain network across frequencies. Besides, these analyses, able to quantify

the individual idiosyncrasies of neural activity, could be extended to clinical settings to provide a more accurate identification of brain connectivity alterations in several disorders, such as dementia due to Alzheimer's disease, schizophrenia, depression, or migraine (Rossini et al., 2020; Bowyer et al., 2015; Dev et al., 2022; Pan et al., 2022).

Furthermore, the CMB algorithm provides a new framework for the characterization of different neural pathologies, as well as to facilitate their diagnosis, thanks to the possibility of studying how they affect to the frequential structure of the functional brain network. The rationale behind the CMB algorithm is in line with the current evolution of science and medicine, which is focused in providing personalized studies, diagnostic tools, and treatments capable of adapting to the particularities of each individual (Goetz and Schork, 2018; Keizer, 2021).

Code availability statement

The code for the computation of the high frequency-resolution connectivity matrices, the Attraction Strength (AS) and the Degree of Dominance (DoD) can be found on Github: <https://github.com/vicrg33/Connectivity-based-Meta-Bands>. The code for the computation of meta-band extraction and the Frequency-Band Activation Sequence (FAS) can be found on Github as well: <https://github.com/pablonuneznovo/Meta-state-extraction-from-high-temporal-resolution-connectivity>. The implementation of the Louvain GJA algorithm used in this study can be found on the brain connectivity toolbox: <https://sites.google.com/site/bctnet/>.

CRedit authorship contribution statement

Víctor Rodríguez-González: Conceptualization, Methodology, Software, Formal analysis, Investigation, Writing – original draft, Visualization, Data curation. **Pablo Núñez:** Methodology, Software, Formal analysis, Writing – review & editing. **Carlos Gómez:** Conceptualization, Methodology, Data curation, Writing – review & editing, Visualization, Supervision. **Yoshihito Shigihara:** Resources, Data curation, Writing – review & editing. **Hideyuki Hoshi:** Resources, Data curation, Writing – review & editing. **Miguel Ángel Tola-Arribas:** Resources, Data curation, Writing – review & editing. **Mónica Cano:** Data curation, Writing – review & editing. **Ángel Guerrero:** Data curation, Writing – review & editing. **David García-Azorín:** Data curation, Writing – review & editing. **Roberto Hornero:** Conceptualization, Writing – review & editing, Supervision, Funding acquisition. **Jesús Poza:** Conceptualization, Methodology, Data curation, Writing – review & editing, Visualization, Supervision, Funding acquisition.

Declaration of competing interest

Hideyuki Hoshi was employed by the company RICOH Company, Ltd. The remaining authors declare no commercial or financial relationships that could be construed as a potential conflict of interest.

Data availability

Data will be made available on request.

Acknowledgements

This research has been funded by “CIBER en Bioingeniería, Biomateriales y Nanomedicina (CIBER-BBN)” through “Instituto de Salud Carlos III” co-funded with ERDF funds. V Rodríguez-González was in receipt of a PIF-UVa grant from the “University of Valladolid”. P. Núñez was funded by the ERA-Net FLAG-ERA JTC2021 project ModelDXConsciousness (Human Brain Project Partnering Project).

Appendix A. Supplementary data

Supplementary material related to this article can be found online at <https://doi.org/10.1016/j.neuroimage.2023.120332>.

References

- Ahlfors, S.P., Han, J., Belliveau, J.W., Hämäläinen, M.S., 2010. Sensitivity of MEG and EEG to source orientation. *Brain Topogr.* 23, 227–232. <https://doi.org/10.1007/s10548-010-0154-x>, URL <http://link.springer.com/10.1007/s10548-010-0154-x>.
- Babiloni, C., Marzano, N., Infarinato, F., Iacono, M., Rizza, G., Aschieri, P., Cibelli, G., Soricelli, A., Eusebi, F., Del Percio, C., 2010. “Neural efficiency” of experts brain during judgment of actions: A high-resolution EEG study in elite and amateur karate athletes. *Behav. Brain Res.* 207 (2), 466–475. <https://doi.org/10.1016/j.bbr.2009.10.034>, URL <https://linkinghub.elsevier.com/retrieve/pii/S0166432809006573>.
- Babiloni, C., Pizzella, V., Gratta, C.D., Ferretti, A., Romani, G.L., 2009. Fundamentals of electroencephalography, magnetoencephalography, and functional magnetic resonance imaging. *Int. Rev. Neurobiol.* 86 (5), 67–80. [https://doi.org/10.1016/S0074-7742\(09\)86005-4](https://doi.org/10.1016/S0074-7742(09)86005-4).
- Baker, A.P., Brookes, M.J., Rezek, I.A., Smith, S.M., Behrens, T., Probert Smith, P.J., Woolrich, M., 2014. Fast transient networks in spontaneous human brain activity. *eLife* 3, <https://doi.org/10.7554/eLife.01867>, URL <https://elifesciences.org/articles/01867>.
- Bassett, D.S., Bullmore, E., 2006. Small-world brain networks. *The Neuroscientist* 12 (6), 512–523. <https://doi.org/10.1177/1073858406293182>.
- Bassett, D.S., Meyer-Lindenberg, A., Achard, S., Duke, T., Bullmore, E., 2006. Adaptive reconfiguration of fractal small-world human brain functional networks. *Proc. Natl. Acad. Sci.* 103, 19518–19523. <https://doi.org/10.1073/pnas.0606005103>.
- Basti, A., Nili, H., Hauk, O., Marzetti, L., Henson, R.N., 2020. Multi-dimensional connectivity: A conceptual and mathematical review. *NeuroImage* 221 (117179), 117179. <https://doi.org/10.1016/j.neuroimage.2020.117179>, <https://linkinghub.elsevier.com/retrieve/pii/S1053811920306650>, <http://www.ncbi.nlm.nih.gov/pubmed/32682988>.
- Bastos, A.M., Schoffelen, J.-M., 2016. A tutorial review of functional connectivity analysis methods and their interpretational pitfalls. *Front. Syst. Neurosci.* 9 (175), 1–23. <https://doi.org/10.3389/fnsys.2015.00175>.
- Bazanov, O., 2012. Comments for current interpretation EEG alpha activity: A review and analysis. *J. Behav. Brain Sci.* 02 (02), 239–248. <https://doi.org/10.4236/jbbs.2012.22027>, URL <http://www.scirp.org/journal/doi.aspx?DOI=10.4236/jbbs.2012.22027>.
- Berger, H., 1934. Über das elektroencephalogramm des menschen. *DMW - Deutsche Med. Wochenschrift* 60 (51), 1947–1949. <https://doi.org/10.1055/s-0028-1130334>, URL <http://www.thieme-connect.de/DOI/DOI?10.1055/s-0028-1130334>.
- Blondel, V.D., Guillaume, J.-L., Lambiotte, R., Lefebvre, E., 2008. Fast unfolding of communities in large networks. *J. Stat. Mech. Theory Exp.* 2008 (10), P10008. <https://doi.org/10.1088/1742-5468/2008/10/P10008>, URL <https://iopscience.iop.org/article/10.1088/1742-5468/2008/10/P10008>.
- Bola, M., Sabel, B.A., 2015. Dynamic reorganization of brain functional networks during cognition. *NeuroImage* 114, 398–413. <https://doi.org/10.1016/j.neuroimage.2015.03.057>.
- Boon, L.I., Geraedts, V.J., Hillebrand, A., Tannemaat, M.R., Contarino, M.F., Stam, C.J., Berendse, H.W., 2019. A systematic review of MEG-based studies in Parkinson’s disease: The motor system and beyond. *Human Brain Mapp.* 40, 2827–2848. <https://doi.org/10.1002/hbm.24562>.
- Boon, L.I., Tewarie, P., Berendse, H.W., Stam, C.J., Hillebrand, A., 2021. Longitudinal consistency of source-space spectral power and functional connectivity using different magnetoencephalography recording systems. *Sci. Rep.* 11 (1), 16336. <https://doi.org/10.1038/s41598-021-95363-2>, <https://www.nature.com/articles/s41598-021-95363-2>.
- Borghini, G., Aricò, P., Di Flumeri, G., Sciaraffa, N., Babiloni, F., 2019. Correlation and similarity between cerebral and non-cerebral electrical activity for user’s states assessment. *Sensors* 19 (3), 704. <https://doi.org/10.3390/s19030704>, URL <http://www.mdpi.com/1424-8220/19/3/704>.
- Bowyer, S.M., Gjini, K., Zhu, X., Kim, L., Moran, J.E., Rizvi, S.U., Gumenyuk, V., Tepley, N., Boutros, N.N., 2015. Potential biomarkers of schizophrenia from MEG resting-state functional connectivity networks: Preliminary data. *J. Behav. Brain Sci.* 05 (01), 1–11. <https://doi.org/10.4236/jbbs.2015.51001>, URL <http://www.scirp.org/journal/doi.aspx?DOI=10.4236/jbbs.2015.51001>.
- Briels, C.T., Briels, C.T., Schoonhoven, D.N., Schoonhoven, D.N., Stam, C.J., De Waal, H., Scheltens, P., Gouw, A.A., 2020. Reproducibility of EEG functional connectivity in Alzheimer’s disease. *Alzheimer’s Res. Therapy* 12 (1), 1–14. <https://doi.org/10.1186/s13195-020-00632-3>, URL <https://alzres.biomedcentral.com/articles/10.1186/s13195-020-00632-3>.
- Brookes, M.J., O’Neill, G.C., Hall, E.L., Woolrich, M.W., Baker, A., Palazzo Corner, S., Robson, S.E., Morris, P.G., Barnes, G.R., 2014. Measuring temporal, spectral and spatial changes in electrophysiological brain network connectivity. *NeuroImage* 91, 282–299. <https://doi.org/10.1016/j.neuroimage.2013.12.066>.
- Brookes, M., Woolrich, M., Barnes, G., 2012. Measuring functional connectivity in MEG: A multivariate approach insensitive to linear source leakage. *NeuroImage* 63, 910–920. <https://doi.org/10.1016/j.neuroimage.2012.03.048>.
- Bullmore, E., Sporns, O., 2009. Complex brain networks: Graph theoretical analysis of structural and functional systems. *Nat. Rev. Neurosci.* 10, 186–198. <https://doi.org/10.1038/nrn2575>.
- Bullmore, E., Sporns, O., 2012. The economy of brain network organization. *Nat. Rev. Neurosci.* 13, 336–349. <https://doi.org/10.1038/nrn3214>.
- Buzsáki, G., Draguhn, A., 2004. Neuronal oscillations in cortical networks. *Science* 304 (5679), 1926–1929. <https://doi.org/10.1126/science.1099745>, URL <https://www.science.org/doi/10.1126/science.1099745>.
- Cabral, J., Vidaurre, D., Marques, P., Magalhães, R., Silva Moreira, P., Miguel Soares, J., Deco, G., Sousa, N., Kringelbach, M.L., 2017. Cognitive performance in healthy older adults relates to spontaneous switching between states of functional connectivity during rest. *Sci. Rep.* 7 (1), 5135. <https://doi.org/10.1038/s41598-017-05425-7>, URL <http://www.nature.com/articles/s41598-017-05425-7>.
- Caspers, J., Rubbert, C., Eickhoff, S.B., Hoffstaedter, F., Südmeyer, M., Hartmann, C.J., Sigl, B., Teichert, N., Aissa, J., Turowski, B., Schnitzler, A., Mathys, C., 2021. Within- and across-network alterations of the sensorimotor network in Parkinson’s disease. *Neuroradiology* 63, 2073–2085. <https://doi.org/10.1007/s00234-021-02731-w>.
- Cassani, R., Estarellas, M., San-Martin, R., Fraga, F.J., Falk, T.H., 2018. Systematic review on resting-state EEG for Alzheimer’s disease diagnosis and progression assessment. *Disease Markers* 2018, 1–26. <https://doi.org/10.1155/2018/5174815>, URL <https://www.hindawi.com/journals/dm/2018/5174815/>.
- Chenji, S., Jha, S., Lee, D., Brown, M., Seres, P., Mah, D., Kalra, S., 2016. Investigating default mode and sensorimotor network connectivity in amyotrophic lateral sclerosis. *PLoS One* 11, e0157443. <https://doi.org/10.1371/journal.pone.0157443>.
- Cho, R.Y., Walker, C.P., Polizzotto, N.R., Wozny, T.A., Fissell, C., Chen, C.-M.A., Lewis, D.A., 2015. Development of sensory Gamma oscillations and cross-frequency coupling from childhood to early adulthood. *Cerebral Cortex* 25 (6), 1509–1518. <https://doi.org/10.1093/cercor/bht341>, URL <https://academic.oup.com/cercor/article-lookup/doi/10.1093/cercor/bht341>.
- Cohen, M.X., 2014. Analyzing Neural Time Series Data: Theory and Practice, first ed. The MIT Press, London, p. 578. [arXiv:arXiv:1011.1669v3](https://arxiv.org/abs/1011.1669v3).
- Cohen, M.X., 2021. A data-driven method to identify frequency boundaries in multichannel electrophysiology data. *J. Neurosci. Methods* 347 (October 2020), 108949. <https://doi.org/10.1016/j.jneumeth.2020.108949>, <https://linkinghub.elsevier.com/retrieve/pii/S0165027020303721>.
- Colclough, G., Woolrich, M., Tewarie, P., Brookes, M., Quinn, A., Smith, S., 2016. How reliable are MEG resting-state connectivity metrics? *NeuroImage* 138, 284–293. <https://doi.org/10.1016/j.neuroimage.2016.05.070>.
- Culham, J.C., Kanwisher, N.G., 2001. Neuroimaging of cognitive functions in human parietal cortex. *Curr. Opin. Neurobiol.* 11, 157–163. [https://doi.org/10.1016/S0959-4388\(00\)00191-4](https://doi.org/10.1016/S0959-4388(00)00191-4).
- Demuru, M., Cava, S.M.L., Pani, S.M., Fraschini, M., 2020. A comparison between power spectral density and network metrics: An EEG study. *Biomed. Signal Process. Control* 57, 101760. <https://doi.org/10.1016/j.bspc.2019.101760>.
- Desikan, R.S., Ségonne, F., Fischl, B., Quinn, B.T., Dickerson, B.C., Blacker, D., Buckner, R.L., Dale, A.M., Maguire, R.P., Hyman, B.T., Albert, M.S., Killiany, R.J., 2006. An automated labeling system for subdividing the human cerebral cortex on MRI scans into gyral based regions of interest. *NeuroImage* 31 (3), 968–980. <https://doi.org/10.1016/j.neuroimage.2006.01.021>.
- Dev, A., Roy, N., Islam, M.K., Biswas, C., Ahmed, H.U., Amin, M.A., Sarker, F., Vaidyanathan, R., Mamun, K.A., 2022. Exploration of EEG-based depression biomarkers identification techniques and their applications: A systematic review. *IEEE Access* 10, 16756–16781. <https://doi.org/10.1109/ACCESS.2022.3146711>, URL <https://ieeexplore.ieee.org/document/9693921/>.
- Douw, L., Nieboer, D., Stam, C.J., Tewarie, P., Hillebrand, A., 2018. Consistency of magnetoencephalographic functional connectivity and network reconstruction using a template versus native MRI for co-registration. *Human Brain Mapp.* 39 (1), 104–119. <https://doi.org/10.1002/hbm.23827>.
- Fan, L., 2021. Mapping the human brain: What is the next frontier? *The Innovation* 2 (1), 100073. <https://doi.org/10.1016/j.xinn.2020.100073>, URL <https://linkinghub.elsevier.com/retrieve/pii/S26667582030076X>.
- Farahibozorg, S.-R., Henson, R.N., Hauk, O., 2018. Adaptive cortical parcellations for source reconstructed EEG/MEG connectomes. *NeuroImage* 169, 23–45. <https://doi.org/10.1016/j.neuroimage.2017.09.009>, URL <https://linkinghub.elsevier.com/retrieve/pii/S1053811917307474>.
- Fauchon, C., Kim, J.A., El-Sayed, R., Osborne, N.R., Rogachov, A., Cheng, J.C., Hemington, K.S., Bosma, R.L., Dunkley, B.T., Oh, J., Bhatia, A., Inman, R.D., Davis, K.D., 2022. A hidden Markov model reveals magnetoencephalography spectral frequency-specific abnormalities of brain state power and phase-coupling in neuropathic pain. *Commun. Biol.* 5, <https://doi.org/10.1038/s42003-022-03967-9>, <https://www.ncbi.nlm.nih.gov/pmc/articles/PMC9492713/>, <https://www.ncbi.nlm.nih.gov/pmc/articles/PMC9492713/?report=abstract>. <https://www.ncbi.nlm.nih.gov/pmc/articles/PMC9492713/>.
- Feher, J., 2012. Quantitative Human Physiology: An Introduction, second ed. Academic Press, London, United Kingdom, pp. 321–331.

- Fellows, L.K., Farah, M.J., 2007. The role of ventromedial prefrontal cortex in decision making: Judgment under uncertainty or judgment per se? *Cerebral Cortex* (New York, N.Y. : 1991) 17, 2669–2674. <http://dx.doi.org/10.1093/CERCOR/BHL176>, URL <https://pubmed.ncbi.nlm.nih.gov/17259643/>.
- Florin, E., Baillet, S., 2015. The brain's resting-state activity is shaped by synchronized cross-frequency coupling of neural oscillations. *NeuroImage* 111, 26–35. <http://dx.doi.org/10.1016/j.neuroimage.2015.01.054>.
- Fonov, V.S., Evans, A.C., McKinstry, R.C., Almlí, C.R., Collins, D.L., 2009. Unbiased nonlinear average age-appropriate brain templates from birth to adulthood. *NeuroImage* 47, S102. [http://dx.doi.org/10.1016/S1053-8119\(09\)70884-5](http://dx.doi.org/10.1016/S1053-8119(09)70884-5).
- Fred, A.L., Kumar, S.N., Haridhas, A.K., Ghosh, S., Bhuvana, H.P., Sim, W.K.J., Vimalan, V., Givo, F.A.S., Jousmäki, V., Padmanabhan, P., Gulyás, B., 2022. A brief introduction to magnetoencephalography (MEG) and its clinical applications. *Brain Sci.* 12, 788. <http://dx.doi.org/10.3390/brainsci12060788>.
- Gates, K.M., Henry, T., Steinley, D., Fair, D.A., 2016. A Monte Carlo evaluation of weighted community detection algorithms. *Front. Neuroinform.* 10 (NOV), 1–16. <http://dx.doi.org/10.3389/fninf.2016.00045>.
- Goetz, L.H., Schork, N.J., 2018. Personalized medicine: Motivation, challenges, and progress. *Fertil. Steril.* 109 (6), 952–963. <http://dx.doi.org/10.1016/j.fertnstert.2018.05.006>, URL <https://linkinghub.elsevier.com/retrieve/pii/S0015028218304072>.
- Gramfort, A., Papadopoulos, T., Olivi, E., Clerc, M., 2010. OpenMEEG: Opensource software for quasistatic bioelectromagnetics. *BioMed. Eng. OnLine* 9 (1), 45. <http://dx.doi.org/10.1186/1475-925X-9-45>.
- Händel, B., Haarmeier, T., 2009. Cross-frequency coupling of brain oscillations indicates the success in visual motion discrimination. *NeuroImage* 45 (3), 1040–1046. <http://dx.doi.org/10.1016/j.neuroimage.2008.12.013>, URL <https://linkinghub.elsevier.com/retrieve/pii/S1053811908012718>.
- Hauk, O., Stenroos, M., Treder, M.S., 2022. Towards an objective evaluation of EEG/MEG source estimation methods – The linear approach. *NeuroImage* 255, 119177. <http://dx.doi.org/10.1016/j.neuroimage.2022.119177>, URL <https://linkinghub.elsevier.com/retrieve/pii/S1053811922002993>.
- He, B., Astolfi, L., Valdes-Sosa, P.A., Marinazzo, D., Palva, S.O., Benar, C.-G., Michel, C.M., Koenig, T., 2019. Electrophysiological brain connectivity: Theory and implementation. *IEEE Trans. Biomed. Eng.* 66, 2115–2137. <http://dx.doi.org/10.1109/TBME.2019.2913928>.
- Hillebrand, A., Barnes, G.R., Bosboom, J.L., Berendse, H.W., Stam, C.J., 2012. Frequency-dependent functional connectivity within resting-state networks: An atlas-based MEG beamformer solution. *NeuroImage* 59 (4), 3909–3921. <http://dx.doi.org/10.1016/j.neuroimage.2011.11.005>, URL <https://linkinghub.elsevier.com/retrieve/pii/S1053811911012845>.
- Hindriks, R., Adhikari, M., Murayama, Y., Ganzetti, M., Mantini, D., Logothetis, N., Deco, G., 2016. Can sliding-window correlations reveal dynamic functional connectivity in resting-state fMRI? *NeuroImage* 127, 242–256. <http://dx.doi.org/10.1016/j.neuroimage.2015.11.055>.
- Hipp, J.F., Hawellek, D.J., Corbetta, M., Siegel, M., Engel, A.K., 2012. Large-scale cortical correlation structure of spontaneous oscillatory activity. *Nature Neurosci.* 15, 884–890. <http://dx.doi.org/10.1038/NN.3101>, <https://pubmed.ncbi.nlm.nih.gov/23861400/>, <https://www.ncbi.nlm.nih.gov/pmc/articles/PMC3861400/>, <https://www.ncbi.nlm.nih.gov/pmc/articles/PMC3861400/?report=abstract>.
- Huang, D., Pipa, G., 2007. Achieving synchronization of networks by an auxiliary hub. *Europhys. Lett.* (EPL) 77 (5), 50010. <http://dx.doi.org/10.1209/0295-5075/77/50010>, URL <https://iopscience.iop.org/article/10.1209/0295-5075/77/50010>.
- Illman, M., Laaksonen, K., Liljeström, M., Jousmäki, V., Piitulainen, H., Forss, N., 2020. Comparing MEG and EEG in detecting the 20-Hz rhythm modulation to tactile and proprioceptive stimulation. *NeuroImage* 215, 116804. <http://dx.doi.org/10.1016/j.neuroimage.2020.116804>.
- Jasper, H.H., Andrews, H.L., 1936. Human brain rhythms: I. Recording techniques and preliminary results. *J. General Psychol.* 14 (1), 98–126. <http://dx.doi.org/10.1080/00221309.1936.9713141>, URL <http://www.tandfonline.com/doi/abs/10.1080/00221309.1936.9713141>.
- Jasper, H.H., Andrews, H.L., 1938. Electro-encephalography: III. Normal differentiation of occipital and precentral regions in man. *Arch. Neurol. Psychiatry* 39 (1), 96–115. <http://dx.doi.org/10.1001/archneurpsyc.1938.02270010106010>.
- Keizer, A.W., 2021. Standardization and personalized medicine using quantitative EEG in clinical settings. *Clin. EEG Neurosci.* 52 (2), 82–89. <http://dx.doi.org/10.1177/1550059419874945>, URL <http://journals.sagepub.com/doi/10.1177/1550059419874945>.
- Khadem, A., Hossein-Zadeh, G.-A., 2014. Quantification of the effects of volume conduction on the EEG/MEG connectivity estimates: An index of sensitivity to brain interactions. *Physiol. Meas.* 35 (10), 2149–2164. <http://dx.doi.org/10.1088/0967-3334/35/10/2149>, URL <https://iopscience.iop.org/article/10.1088/0967-3334/35/10/2149>.
- Khambhati, A.N., Sizemore, A.E., Betzel, R.F., Bassett, D.S., 2018. Modeling and interpreting mesoscale network dynamics. *NeuroImage* 180, 337–349. <http://dx.doi.org/10.1016/j.neuroimage.2017.06.029>.
- Lai, M., Demuru, M., Hillebrand, A., Fraschini, M., 2018. A comparison between scalp- and source-reconstructed EEG networks. *Sci. Rep.* 8 (1), 12269. <http://dx.doi.org/10.1038/s41598-018-30869-w>.
- Larson-Prior, L., Oostenveld, R., Della Penna, S., Michalareas, G., Prior, F., Babajani-Feremi, A., Schoffelen, J.-M., Marzetti, L., de Pasquale, F., Di Pompeo, F., Stout, J., Woolrich, M., Luo, Q., Bucholz, R., Fries, P., Pizzella, V., Romani, G., Corbetta, M., Snyder, A., 2013. Adding dynamics to the human connectome project with MEG. *NeuroImage* 80, 190–201. <http://dx.doi.org/10.1016/j.neuroimage.2013.05.056>.
- Lin, F.H., Witzel, T., Ahlfors, S.P., Stufflebeam, S.M., Belliveau, J.W., Hämäläinen, M.S., 2006. Assessing and improving the spatial accuracy in MEG source localization by depth-weighted minimum-norm estimates. *NeuroImage* 31 (1), 160–171. <http://dx.doi.org/10.1016/j.neuroimage.2005.11.054>.
- Little, S., Bonaiuto, J., Barnes, G., Bestmann, S., 2019. Human motor cortical beta bursts relate to movement planning and response errors. *PLoS Biol.* 17, <http://dx.doi.org/10.1371/JOURNAL.PBIO.3000479>, <https://pubmed.ncbi.nlm.nih.gov/310548011-0202-1/>, <https://www.ncbi.nlm.nih.gov/pmc/articles/PMC6795457/>, <https://www.ncbi.nlm.nih.gov/pmc/articles/PMC6795457/?report=abstract>.
- Lopes, F., 2013. EEG and MEG : Relevance to Neuroscience. *Neuron* 80 (5), 1112–1128. <http://dx.doi.org/10.1016/j.neuron.2013.10.017>.
- Malmivuo, J., 2012. Comparison of the properties of EEG and MEG in detecting the electric activity of the brain. *Brain Topogr.* 25, 1–19. <http://dx.doi.org/10.1007/s10548-011-0202-1>, URL <http://link.springer.com/10.1007/s10548-011-0202-1>.
- Marwan, N., Carmen Romano, M., Thiel, M., Kurths, J., 2007. Recurrence plots for the analysis of complex systems. *Phys. Rep.* 438 (5–6), 237–329. <http://dx.doi.org/10.1016/j.physrep.2006.11.001>.
- Mennigen, E., Miller, R.L., Rashid, B., Fryer, S.L., Loewy, R.L., Stuart, B.K., Mathalon, D.H., Calhoun, V.D., 2018. Reduced higher-dimensional resting state fMRI dynamism in clinical high-risk individuals for schizophrenia identified by meta-state analysis. *Schizophrenia Res.* 201, 217. <http://dx.doi.org/10.1016/J.SCHRES.2018.06.007>, <https://pubmed.ncbi.nlm.nih.gov/310548011-0202-1/>, <https://www.ncbi.nlm.nih.gov/pmc/articles/PMC6252113/>, <https://www.ncbi.nlm.nih.gov/pmc/articles/PMC6252113/?report=abstract>.
- Millett, D., 2001. Hans Berger: From psychic energy to the EEG. *Perspect. Biol. Med.* 44, 522–542. <http://dx.doi.org/10.1353/PBM.2001.0070>, URL <https://muse.jhu.edu/article/26086>.
- Miraglia, F., Vecchio, F., Rossini, P.M., 2017. Searching for signs of aging and dementia in EEG through network analysis. *Behav. Brain Res.* 317 (1), 292–300. <http://dx.doi.org/10.1016/j.bbr.2016.09.057>.
- Molins, A., Stufflebeam, S., Brown, E., Hämäläinen, M., 2008. Quantification of the benefit from integrating MEG and EEG data in minimum l2-norm estimation. *NeuroImage* 42, 1069–1077. <http://dx.doi.org/10.1016/j.neuroimage.2008.05.064>.
- Mutanen, T.P., Metsomaa, J., Liljander, S., Ilmoniemi, R.J., 2018. Automatic and robust noise suppression in EEG and MEG: The SOUND algorithm. *NeuroImage* 166, 135–151. <http://dx.doi.org/10.1016/j.neuroimage.2017.10.021>.
- Newson, J.J., Thiagarajan, T.C., 2019. EEG frequency bands in psychiatric disorders: A review of resting state studies. *Front. Hum. Neurosci.* 12 (521), 1–24. <http://dx.doi.org/10.3389/fnhum.2018.00521>, URL <https://www.frontiersin.org/article/10.3389/fnhum.2018.00521/full>.
- Núñez, P., Gómez, C., Rodríguez-González, V., Hillebrand, A., Tewarie, P., Gomez-Pilar, J., Molina, V., Hornero, R., Poza, J., 2022. Schizophrenia induces abnormal frequency-dependent patterns of dynamic brain network reconfiguration during an auditory oddball task. *J. Neural Eng.* 19 (1), 016033. <http://dx.doi.org/10.1088/1741-2552/ac514e>, URL <https://iopscience.iop.org/article/10.1088/1741-2552/ac514e>.
- Núñez, P., Poza, J., Gómez, C., Rodríguez-González, V., Hillebrand, A., Tewarie, P., Tola-Arribas, M.Á., Cano, M., Hornero, R., 2021. Abnormal meta-state activation of dynamic brain networks across the Alzheimer spectrum. *NeuroImage* 232, 117898. <http://dx.doi.org/10.1016/j.neuroimage.2021.117898>.
- O'Neill, G.C., Tewarie, P., Vidaurre, D., Lüuzzi, L., Woolrich, M.W., Brookes, M.J., 2018. Dynamics of large-scale electrophysiological networks: A technical review. *NeuroImage* 180, 559–576. <http://dx.doi.org/10.1016/j.neuroimage.2017.10.003>, URL <https://linkinghub.elsevier.com/retrieve/pii/S1053811917308169>.
- O'Reilly, C., Elsabbagh, M., 2021. Intracranial recordings reveal ubiquitous in-phase and anti-phase functional connectivity between homotopic brain regions in humans. *J. Neurosci. Res.* 99 (3), 887–897. <http://dx.doi.org/10.1002/jnr.24748>, URL <https://onlinelibrary.wiley.com/doi/10.1002/jnr.24748>.
- O'Reilly, C., Lewis, J.D., Elsabbagh, M., 2017. Is functional brain connectivity atypical in autism? A systematic review of EEG and MEG studies. *PLoS One* 12 (5), e0175870. <http://dx.doi.org/10.1371/journal.pone.0175870>, URL <https://dx.plos.org/10.1371/journal.pone.0175870>.
- Pan, L.-H., Hsiao, F.-J., Chen, W.-T., Wang, S.-J., 2022. Resting state electrophysiological cortical activity: A brain signature candidate for patients with migraine. *Current Pain Headache Rep.* 26 (4), 289–297. <http://dx.doi.org/10.1007/s11916-022-01030-0>, URL <https://link.springer.com/10.1007/s11916-022-01030-0>.
- Pascarelli, M.T., Del Percio, C., De Pandis, M.F., Ferri, R., Lizio, R., Noce, G., Lopez, S., Rizzo, M., Soricelli, A., Nobili, F., Arnaldi, D., Famà, F., Orzi, F., Buttinelli, C., Giubilei, F., Salvetti, M., Cipollini, V., Franciotti, R., Onofri, M., Fuhr, P., Gschwandtner, U., Ransmayr, G., Aarsland, D., Parnetti, L., Farotti, L., Marizzoni, M., D'Antonio, F., De Lena, C., Güntekin, B., Hanoğlu, L., Yener, G., Emek-Savaş, D.D., Triggiani, A.I., Paul Taylor, J., McKeith, I., Stocchi, F., Vacca, L., Hampel, H., Frisoni, G.B., Bonanni, L., Babiloni, C., 2020. Abnormalities of resting-state EEG in patients with prodromal and overt dementia with Lewy bodies: Relation to clinical symptoms. *Clin. Neurophysiol.* 131 (11), 2716–2731. <http://dx.doi.org/10.1016/j.clinph.2020.08.011>.

- [//dx.doi.org/10.1016/j.clinph.2020.09.004](https://doi.org/10.1016/j.clinph.2020.09.004), URL <https://linkinghub.elsevier.com/retrieve/pii/S1388245720304752>.
- Pascual-Marqui, R.D., 2002. Standardized low-resolution brain electromagnetic tomography (sLORETA): Technical details. *Methods Find. Exp. Clin. Pharmacol.* 24 Suppl D, 5–12.
- Perez, M.A., Cohen, L.G., 2009. Interhemispheric inhibition between primary motor cortices: What have we learned? *J. Physiol.* 587 (4), 725–726. <http://dx.doi.org/10.1113/jphysiol.2008.166926>, URL <http://doi.wiley.com/10.1113/jphysiol.2008.166926>.
- Ponce-Alvarez, A., Deco, G., Hagmann, P., Romani, G.L., Mantini, D., Corbetta, M., 2015. Resting-state temporal synchronization networks emerge from connectivity topology and heterogeneity. *PLoS Comput. Biol.* 11 (2), 1–23. <http://dx.doi.org/10.1371/journal.pcbi.1004100>.
- Poza, J., Gómez, C., García, M., Tola-Arribas, M.A., Carreres, A., Cano, M., Hornero, R., 2017. Spatio-temporal fluctuations of neural dynamics in mild cognitive impairment and Alzheimer's Disease. *Current Alzheimer Res.* 14 (9), <http://dx.doi.org/10.2174/1567205014666170309115656>, URL <http://www.eurekaselect.com/150776/article>.
- Prichard, D., Theiler, J., 1994. Generating surrogate data for time series with several simultaneously measured variables. *Phys. Rev. Lett.* 73 (7), 951–954. <http://dx.doi.org/10.1103/PhysRevLett.73.951>.
- Puxeddu, M.G., Petti, M., Astolfi, L., 2021. Multi-layer analysis of multi-frequency brain networks as a new tool to study EEG topological organization *. In: 43rd Annual International Conference of the IEEE Engineering in Medicine and Biology Society. EMBC, IEEE, Online, pp. 924–927.
- Rahimi, S., Jackson, R., Farahibozorg, S.-R., Hauk, O., 2023. Time-lagged multidimensional pattern connectivity (TL-MDPC): An EEG/MEG pattern transformation based functional connectivity metric. *NeuroImage* 270, 119958. <http://dx.doi.org/10.1016/j.neuroimage.2023.119958>, URL <https://linkinghub.elsevier.com/retrieve/pii/S1053811923001040>.
- Raichle, M.E., MacLeod, A.M., Snyder, A.Z., Powers, W.J., Gusnard, D.A., Shulman, G.L., 2001. A default mode of brain function. *Proc. Natl. Acad. Sci.* 98, 676–682. <http://dx.doi.org/10.1073/pnas.98.2.676>.
- Raichle, M.E., Snyder, A.Z., 2007. A default mode of brain function: A brief history of an evolving idea. *NeuroImage* 37, 1083–1090. <http://dx.doi.org/10.1016/j.NEUROIMAGE.2007.02.041>.
- Ramirez-Mahaluf, J.P., Medel, V., Tepper, Á., Alliende, L.M., Sato, J.R., Ossandon, T., Crossley, N.A., 2020. Transitions between human functional brain networks reveal complex, cost-efficient and behaviorally-relevant temporal paths. *NeuroImage* 219, <http://dx.doi.org/10.1016/j.NEUROIMAGE.2020.117027>, URL <https://pubmed.ncbi.nlm.nih.gov/32522663/>.
- Rammpp, S., Stefan, H., 2007. On the opposition of EEG and MEG. *Clin. Neurophysiol.* 118 (8), 1658–1659. <http://dx.doi.org/10.1016/j.clinph.2007.04.021>, URL <https://linkinghub.elsevier.com/retrieve/pii/S1388245707001952>.
- Riddle, J., McFerren, A., Frohlich, A., Frohlich, J., 2021. Causal role of cross-frequency coupling in distinct components of cognitive control. *Progress Neurobiol.* 202, 102033. <http://dx.doi.org/10.1016/j.pneurobio.2021.102033>, URL <https://linkinghub.elsevier.com/retrieve/pii/S0301008221000472>.
- Rizkallah, J., Amoud, H., Fraschini, M., Wendling, F., Hassan, M., 2020. Exploring the correlation between M/EEG source-space and fMRI networks at rest. *Brain Topogr.* 33 (2), 151–160. <http://dx.doi.org/10.1007/s10548-020-00753-w>.
- Rodríguez-González, V., Gómez, C., Shighihara, Y., Hoshi, H., Revilla-Vallejo, M., Hornero, R., Poza, J., 2020. Consistency of local activation parameters at sensor and source-level in neural signals. *J. Neural Eng.* 17 (5), 056020. <http://dx.doi.org/10.1088/1741-2552/abb582>.
- Rodríguez-González, V., Gutiérrez-de Pablo, V., Gómez, C., Shighihara, Y., Hoshi, H., Hornero, R., Tola-Arribas, M.Á., Cano, M., Poza, J., 2021. High frequential resolution networks: Considerations on a new functional brain connectivity framework. In: 43rd Annual International Conference of the IEEE Engineering in Medicine & Biology Society. IEEE, Online, pp. 722–725.
- Rodríguez-González, V., Poza, J., Núñez, P., Gómez, C., García, M., Shighihara, Y., Hoshi, H., Santamaría-Vázquez, E., Hornero, R., 2019. Towards automatic artifact rejection in resting-state MEG recordings: Evaluating the performance of the SOUND algorithm. In: 2019 41st Annual International Conference of the IEEE Engineering in Medicine and Biology Society. EMBC, IEEE, Berlin (Deutschland), pp. 4807–4810. <http://dx.doi.org/10.1109/EMBC.2019.8856587>.
- Rossini, P., Di Iorio, R., Vecchio, F., Anfossi, M., Babiloni, C., Bozzali, M., Bruni, A., Cappa, S., Escudero, J., Fraga, F., Giannakopoulos, P., Guntekin, B., Logroscino, G., Marra, C., Miraglia, F., Panza, F., Tecchio, F., Pascual-Leone, A., Dubois, B., 2020. Early diagnosis of Alzheimer's disease: The role of biomarkers including advanced EEG signal analysis. Report from the IFCN-sponsored panel of experts. *Clin. Neurophysiol.* 131 (6), 1287–1310. <http://dx.doi.org/10.1016/j.clinph.2020.03.003>, URL <https://linkinghub.elsevier.com/retrieve/pii/S1388245720300870>.
- Rubinow, M., Sporns, O., 2011. Weight-conserving characterization of complex functional brain networks. *NeuroImage* 56 (4), 2068–2079. <http://dx.doi.org/10.1016/j.neuroimage.2011.03.069>, URL <https://linkinghub.elsevier.com/retrieve/pii/S105381191100348X>.
- Sanei, S., Chambers, J., 2021. EEG Signal Processing & Machine Learning, second ed. John Wiley and Sons Ltd., West Sussex, England, p. 752.
- Sasai, S., Homae, F., Watanabe, H., Sasaki, A.T., Tanabe, H.C., Sadato, N., Taga, G., 2014. Frequency-specific network topologies in the resting human brain. *Front. Hum. Neurosci.* 8, <http://dx.doi.org/10.3389/fnhum.2014.01022>.
- Schoffelen, J.-M., Gross, J., 2009. Source connectivity analysis with MEG and EEG. *Human Brain Mapp.* 30 (6), 1857–1865. <http://dx.doi.org/10.1002/hbm.20745>, URL <https://onlinelibrary.wiley.com/doi/10.1002/hbm.20745>.
- Schoonhoven, D.N., Briels, C.T., Hillebrand, A., Scheltens, P., Stam, C.J., Gouw, A.A., 2022. Sensitive and reproducible MEG resting-state metrics of functional connectivity in Alzheimer's disease. *Alzheimer's Res. Therapy* 14 (1), 38. <http://dx.doi.org/10.1186/s13195-022-00970-4>, URL <https://alzres.biomedcentral.com/articles/10.1186/s13195-022-00970-4>.
- Stam, C.J., 2006. *Nonlinear Brain Dynamics*, first ed. Nova Science Publishers, New York, p. 148.
- Stam, C.J., Nolte, G., Daffertshofer, A., 2007. Phase lag index: Assessment of functional connectivity from multi channel EEG and MEG with diminished bias from common sources. *Human Brain Mapp.* 28 (11), 1178–1193. <http://dx.doi.org/10.1002/hbm.20346>, URL <http://doi.wiley.com/10.1002/hbm.20346>.
- Stam, C.J., van Straaten, E.C.W., 2012. The organization of physiological brain networks. *Clin. Neurophysiol.* 123 (6), 1067–1087. <http://dx.doi.org/10.1016/j.clinph.2012.01.011>.
- Stankovski, T., Ticcinelli, V., McClintock, P.V.E., Stefanovska, A., 2017. Neural cross-frequency coupling functions. *Front. Syst. Neurosci.* 11, <http://dx.doi.org/10.3389/fnsys.2017.00033>.
- Tadel, F., Baillet, S., Mosher, J.C., Pantazis, D., Leahy, R.M., 2011. Brainstorm: A user-friendly application for MEG/EEG analysis. *Comput. Intell. Neurosci.* 2011, 1–13. <http://dx.doi.org/10.1155/2011/879716>.
- Tait, L., Özkan, A., Szul, M.J., Zhang, J., 2021. A systematic evaluation of source reconstruction of resting MEG of the human brain with a new high-resolution atlas: Performance, precision, and parcellation. *Human Brain Mapp.* 42 (14), 4685–4707. <http://dx.doi.org/10.1002/hbm.25578>.
- Tewarie, P., Hunt, B.A.E., O'Neill, G.C., Byrne, A., Aquino, K., Bauer, M., Mullinger, K.J., Coombes, S., Brookes, M.J., 2019a. Relationships between neuronal oscillatory amplitude and dynamic functional connectivity. *Cerebral Cortex* 29 (6), 2668–2681. <http://dx.doi.org/10.1093/cercor/bhy136>, URL <https://academic.oup.com/cercor/article/29/6/2668/5036075>.
- Tewarie, P., Luzzi, L., O'Neill, G.C., Quinn, A.J., Griffa, A., Woolrich, M.W., Stam, C.J., Hillebrand, A., Brookes, M.J., 2019b. Tracking dynamic brain networks using high temporal resolution MEG measures of functional connectivity. *NeuroImage* 200, 38–50. <http://dx.doi.org/10.1016/j.neuroimage.2019.06.006>.
- Tognoli, E., Kelso, J.A.S., 2014. The metastable brain. *Neuron* 81 (1), 35–48. <http://dx.doi.org/10.1016/j.neuron.2013.12.022>, URL <https://linkinghub.elsevier.com/retrieve/pii/S0896627313011835>.
- Trajkovic, J., Gregorio, F.D., Ferri, F., Marzi, C., Diciotti, S., Romei, V., 2021. Resting state alpha oscillatory activity is a valid and reliable marker of schizotypy. *Sci. Rep.* 11, 10379. <http://dx.doi.org/10.1038/S41598-021-89690-7>, /pmc/articles/PMC8129121/ /pmc/articles/PMC8129121/?report=abstract. <https://www.ncbi.nlm.nih.gov/pmc/articles/PMC8129121/>.
- Tsapkini, K., Frangakis, C.E., Hillis, A.E., 2011. The function of the left anterior temporal pole: Evidence from acute stroke and infarct volume. *Brain* 134, 3094. <http://dx.doi.org/10.1093/BRAIN/AWR050>, /pmc/articles/PMC3187536/ /pmc/articles/PMC3187536/?report=abstract. <https://www.ncbi.nlm.nih.gov/pmc/articles/PMC3187536/>.
- Uhlhaas, P.J., Haenschel, C., Nikolic, D., Singer, W., 2008. The role of oscillations and synchrony in cortical networks and their putative relevance for the pathophysiology of Schizophrenia. *Schizophrenia Bull.* 34 (5), 927–943. <http://dx.doi.org/10.1093/schbul/sbn062>, URL <https://academic.oup.com/schizophreniabulletin/article-lookup/doi/10.1093/schbul/sbn062>.
- Uhlhaas, P.J., Pipa, G., Lima, B., Melloni, L., Neuenschwander, S., Nikolic, D., Singer, W., 2009. Neural synchrony in cortical networks: History, concept and current status. *Front. Integr. Neurosci.* 3 (JUL), <http://dx.doi.org/10.3389/neuro.07.017.2009>, URL <http://journal.frontiersin.org/article/10.3389/neuro.07.017.2009/abstract>.
- van den Broek, S., Reinders, F., Donderwinkel, M., Peters, M., 1998. Volume conduction effects in EEG and MEG. *Electroencephalogr. Clin. Neurophysiol.* 106, 522–534. [http://dx.doi.org/10.1016/S0013-4694\(97\)00147-8](http://dx.doi.org/10.1016/S0013-4694(97)00147-8).
- Vecchiato, G., Toppi, J., Astolfi, L., De Vico Fallani, F., Cincotti, F., Mattia, D., Bez, F., Babiloni, F., 2011. Spectral EEG frontal asymmetries correlate with the experienced pleasantness of TV commercial advertisements. *Med. Biol. Eng. Comput.* 49 (5), 579–583. <http://dx.doi.org/10.1007/s11517-011-0747-x>, URL <http://link.springer.com/10.1007/s11517-011-0747-x>.
- Vicente, R., Gollo, L.L., Mirasso, C.R., Fischer, I., Pipa, G., 2008. Dynamical relaying can yield zero time lag neuronal synchrony despite long conduction delays. *Proc. Natl. Acad. Sci.* 105 (44), 17157–17162. <http://dx.doi.org/10.1073/pnas.0809353105>, URL <https://pnas.org/doi/full/10.1073/pnas.0809353105>.
- Vidaurre, D., Hunt, L.T., Quinn, A.J., Hunt, B.A., Brookes, M.J., Nobre, A.C., Woolrich, M.W., 2018. Spontaneous cortical activity transiently organises into frequency specific phase-coupling networks. *Nature Commun.* 9, <http://dx.doi.org/10.1038/S41467-018-05316-Z>, /pmc/articles/PMC6065434/ /pmc/articles/PMC6065434/?report=abstract. <https://www.ncbi.nlm.nih.gov/pmc/articles/PMC6065434/>.

- Vidaurre, D., Quinn, A.J., Baker, A.P., Dupret, D., Tejero-Cantero, A., Woolrich, M.W., 2016. Spectrally resolved fast transient brain states in electrophysiological data. *NeuroImage* 126, 81–95. <http://dx.doi.org/10.1016/j.neuroimage.2015.11.047>.
- Vohryzek, J., Deco, G., Cessac, B., Kringelbach, M.L., Cabral, J., 2020. Ghost attractors in spontaneous brain activity: Recurrent excursions into functionally-relevant BOLD phase-locking states. *Front. Syst. Neurosci.* 14 (20), 1–15. <http://dx.doi.org/10.3389/fnsys.2020.00020>, URL <https://www.frontiersin.org/article/10.3389/fnsys.2020.00020/full>.
- von Schwanenflug, N., Ramirez-Mahaluf, J.P., Krohn, S., Romanello, A., Heine, J., Prüss, H., Crossley, N.A., Finke, C., 2023. Reduced resilience of brain state transitions in anti-N-methyl-D-aspartate receptor encephalitis. *Eur. J. Neurosci.* 57, 568–579. <http://dx.doi.org/10.1111/EJN.15901>, <https://onlinelibrary.wiley.com/doi/full/10.1111/ejn.15901>. <https://onlinelibrary.wiley.com/doi/abs/10.1111/ejn.15901>. <https://onlinelibrary.wiley.com/doi/10.1111/ejn.15901>.
- Walter, W., 1936. The location of cerebral tumours by electro-encephalography. *Lancet* 228 (5893), 305–308. [http://dx.doi.org/10.1016/S0140-6736\(01\)05173-X](http://dx.doi.org/10.1016/S0140-6736(01)05173-X), URL <https://linkinghub.elsevier.com/retrieve/pii/S014067360105173X>.
- Walter, W.G., Dovey, V.J., 1944. Electro-encephalography in cases of sub-cortical tumour. *J. Neurol., Neurosurg. Psychiatry* 7 (3–4), 57–65. <http://dx.doi.org/10.1136/jnnp.7.3-4.57>, URL <https://jnnp.bmj.com/lookup/doi/10.1136/jnnp.7.3-4.57>.
- Webber, Jr., C.L., Zbilut, J.P., 2005. Recurrence quantification analysis of nonlinear dynamical systems. In: *Tutorials in Contemporary Nonlinear Methods for the Behavioral Sciences Web Book*, vol. 94, pp. 26–94.
- Zhao, X., Wu, Q., Chen, Y., Song, X., Ni, H., Ming, D., 2019. Hub patterns-based detection of dynamic functional network metastates in resting state: A test-retest analysis. *Front. Neurosci.* 13, <http://dx.doi.org/10.3389/FNINS.2019.00856/FULL>, /pmc/articles/PMC6749078/ /pmc/articles/PMC6749078/?report=abstract. <https://www.ncbi.nlm.nih.gov/pmc/articles/PMC6749078/>.
- Zhou, Q., Zhang, L., Feng, J., Lo, C.-Y.Z., 2019. Tracking the main states of dynamic functional connectivity in resting state. *Front. Neurosci.* 13 (JUL), 1–12. <http://dx.doi.org/10.3389/fnins.2019.00685>.